To appear in *Revista Mexicana de Astronomía y Astrofísica*

arXiv:astro-ph/0211554v1 25 Nov 2002

OPTICAL LINE PROFILE VARIABILITY OF THE B1+NEUTRON STAR BINARY SYSTEM
LS I+65 010 = 2S 0114+650

Gloria Koenigsberger[1,2] Gabriela Canalizo[3] Anabel Arrieta[1] Michael G. Richer[1] Leonid Georgiev[1]

Submitted to RevMexAA 2nd February 2008

RESUMEN

Presentamos los resultados de observaciones espectroscopicas de alta resolución del sistema binario masivo con emision de rayos-X LS I+65 010=2S 0114+650. Se encuentra una correlación entre el ancho equivalente y la velocidad radial de las líneas en absorción tal que las líneas más intensas tienen las velocidades mas grandes. La velocidad del sistema se deduce utilizando las líneas menos intensas, obteniéndose $v_{helio}=-31$km s^{-1}, la cual, si se atribuye unicamente a la rotación Galáctica, implica que LS I+65 010 se ubica a ∼3 kpc del la vecindad solar. Las lineas interestelares de Na I D muestran dos componentes de alta velocidad y dos componentes que se pueden asociar a los brazos espirales de Orion y de Perseo. Se reporta la presencia de variabilidad en los perfiles de las las líneas, y se sugiere que la curva de velocidad radial del sistema está deformada por estas variaciones. Nuestros datos favorecen el periodo orbital P_{orb}=11.591.

ABSTRACT

We present high resolution spectroscopic observations of the massive X-ray binary system LS I+65 010=2S 0114+650 in the optical wavelength region. A correlation between equivalent width and radial velocity of photospheric absorption lines is found. The systemic velocity, inferred from the weaker lines is v_{helio} -31 ± 5 km s^{-1}, which, if attributed solely to the Galactic rotation curve, implies that LS I+65 010 lies within 3 kpc from the Sun. The ISM Na I D lines display 2 resolved high velocity components at v_{helio} -70, -48 km s^{-1}, possibly associated with gas surrounding the binary system, in addition to the -24 -8 km s^{-1} ISM features due to the Orion and in the Perseus arm regions. Strong photospheric line profile variability is present on a night to night timescale, with He I 5875 Å displaying an additional blue-shifted absorption in some of the spectra, similar to what is observed in the optical counterpart of Vela X-1. A connection between the extended blue wing and X-ray maximum is suggested. Short timescale variations in line profiles are detected on only two nights, but the evidence that these variations occur on the 2.78 hour X-ray flaring period is marginal.

Key Words: **MASSIVE X-RAY BINARY SYSTEMS; 2S 0114+650**

1. INTRODUCTION

The study of massive X-ray binary systems (MXRBs) is of significant interest because it provides a wealth of information on a variety of astrophysical problems such as the determination of the masses of the collapsed objects, the mechanisms that lead to the emission of X-rays, the physical processes involved in the production of accretion disks and relativistic jets, and possibly the phenomena that result in some of the observed γ-ray bursts. Progress in solving some of these problems, however, requires precise information of the binary system parameters. In particular, well-determined properties of the normal star in the system are essential. This is, however, not an easy enterprise in most cases due to the effects introduced by the interactions that occur in the system. For example, the X-rays that are produced near the collapsed companion can alter the ioniza-

---

[1] Instituto de Astronomía, UNAM, México D.F. 04510

[2] Centro de Ciencias Físicas, UNAM, México

[3] Institute of Geophysics and Planetary Sciences, Lawrence Livermore National Laboratory

tion structure of the stellar wind of the primary, producing emission that contaminates the photospheric absorption-line spectrum. If the X-ray flux is variable, the absorption line profiles may also reflect this variability. In addition, the presence of a close companion may produce stellar pulsations if the orbital period is not synchronized with the rotational period (Kumar, Ao & Quataert 1995, Witte & Savonije 1999), and such pulsations are expected to produce line-profile variability (Vogt & Penrod 1983). It is therefore of interest to establish the degree to which photospheric lines are altered by the presence of the collapsed companion and hence, detailed studies of individual binary systems are necessary. In this paper we present an analysis of line profile variability in LS I+65 010, the optical counterpart of the intriguing MXRB, 2S0114+650.

First discovered as an X-ray source by SAS-3 in 1977 (Dower et al. 1977), the optical counterpart of 2S0114+650 was identified shortly thereafter (Margon 1977). Its variable star name is V662 Cas (Kholopov et al., 1989). The system is highly reddened, and believed to consist of a B1Ia supergiant (Reig et al. 1996) and a neutron star companion. Since its initial discovery as a binary X-ray source, it has been observed by nearly every X-ray experiment that has been launched. Koenigsberger et al. (1983), carried out a study of the data obtained by the OSO-8, HEAO 1 and EINSTEIN observatories, and discovered the presence of X-ray flaring activity on timescales of ∼3 hours, in addition to smaller amplitude oscillations in the X-ray flux with a period of 894 seconds. The shorter period was initially identified with the period of the X-ray pulsar, but Yamauchi et al. (1990) were not able to confirm this period in data from the Ginga experiment, finding instead evidence for a posible 850 second period. On the other hand, the flaring activity has now been shown to be periodic with P=2.78 hours (Finley et al. 1992; Hall et al. 2000), after combining the data from the earlier observations and from ROSAT, EXOSAT, and RXTE. Finley et al. (1992) suggested that the 2.78 hour period could actually be due to the pulsar's rotation. This, however, would make it an extremely slow pulsar (the slowest X-ray pulsar known to date is ϕ Per, which has a period of ∼15 minutes), especially when compared with many of the X-ray pulsars whose rotation periods are on the order of miliseconds. Li & van den Heuvel (1999) showed that the neutron star could indeed have reduced its rotation rate within the lifetime of the B-supergiant companion, but, to do so, it must have had a very large ($> 10^{14}$ Gauss) magnetic field at the time of its birth. Thus, the new-born pulsar would have been a *magnetar*, objects that are predicted theoretically, but for which few candidates exists as yet (Gotthelf et al. 2002; Marsden et al. 1999).

An alternative scenario for explaining the periodic X-ray flaring activity consists of assuming that the optical counterpart undergoes periodic oscillations and that these oscillations lead to a highly structured stellar wind. As the neutron star accretes from shells of stellar wind with alternating high and low densities, it produces a varying X-ray flux on the same timescale as the stellar oscillations. This suggestion, first presented by Finley et al. (1992), sparked interest in searching for the 2.78 hour periodicity at optical wavelengths. Although Taylor et al. (1995) detected 0.009 mag peak-to-peak periodic photometric variations in the V-band continuum, Finley et al. (1994) and Bell et al. (1993) failed to detect any significant variations. This alternative scenario appears to be less likely than that of the slowly rotating neutron star. In addition to the difficulty in conclusively establishing the presence of periodic variability in the B1-star, there is the problem of being able to show that the stellar oscillations can lead not only to a variable stellar wind, but to a stellar wind that has a *periodic* density structure.

LS I+65 010 presents broad and variable Hα emission (Margon 1980; Liu & Hang 1999; Reig et al. 1996). Crampton et al. (1985) classified the optical component as B0.5, based on spectra obtained in 1978 and 1982-84. They noted, however, the difficulty in determining the luminosity class from the spectrum, since the upper Balmer lines indicate a luminosity class Ia, but the O, N, and Si lines suggest a class III classification, while, assuming it is located in the Perseus spiral arm (∼2.5 kpc), its luminosity would correspond to class II. Aab et al. (1983) proposed that the primary in 2S 0114+650 may be hydrogen-deficient, thus explaining the weaker strengths of the Balmer lines. However, Reig et al. (1996) determined a B1 Ia spectral classification, based on optical spectra and infrared and optical photometry, a classification that is supported by Liu & Hang (1999). Reig et al. (1996) also suggest a larger distance to the system of $\sim 7 \pm 3.6$ kpc. In Table 1 we summarize the parameters that have been derived for this system.

The orbital period was determined by Crampton et al. (1985), who found a very small semi-amplitude (K=17 km s^{-1}) for the B-star's radial velocity variations and they were unable to distinguish between a circular (P=11.591 days) and an eccentric (e=0.16, P=11.588 days) solution for the orbital motion. Recently, Corbet et al. (1999) found evidence for a slightly longer period, 11.63 days (T_0=2450091.36), than that derived by Crampton et al., based on phase-dependent variations in the RXTE observations that are interpreted as eclipses of the X-ray source. This period, however, is not consistent with the optical RV curve of Crampton et al., leading Corbet et al. to conclude that the orbital periods derived from the optical and X-ray measurements are apparently inconsistent, with no explanation yet available for this discrepancy.

In this paper we present the analysis of optical spectra of LS I +65 010 obtained in 1993, 1995 and 2001 with the objective of studying the B1-star's spectral variability. The goals of this paper are to establish limits on the amplitudes and nature of line profile variability, and to search for periodicity, on the 2.78 hour X-ray flaring period, which would connect the X-ray behavior with possible oscillations in the B1-star. The absence of these oscillations would support the scenario that the neutron star in 2S 0114+650 was born as a magnetar.

2. OBSERVATIONS AND DATA REDUCTION

Seven sets of observations of LS I+65 010, summarized in Table 2, were obtained between 1993 and 2001. Three sets (1993 October 9, 10 and 13 (UT)) were obtained using the REOSC echelle with the 2.1 m telescope of the Observatorio Astronómico Nacional de San Pedro Martir (OAN/SPM) and with the camera system described by Diego & Echevarria (1994). A 1024 × 1024 Photometrics CCD detector was used, having pixel size of 19 μm. With the 300 grooves mm^{-1} echellete, the system gives a resolution of of 7.8 Å mm^{-1} (0.15 Å pixel^{-1}) at H β and 10.7 Å mm^{-1} (0.20 Å pixel^{-1}) at Hα. The resolution is R=17,000, which corresponds to 17 km s^{-1} per 2 pixels. The slit was set at a width of 150 μm, which corresponds to 2″. Each night, a sequence of bias frames was obtained at the beginning and at the end of the night, as well as sequences of lamp flat fields. The target star was observed with 15 or 30 minute exposure times, in a sequence of 3 or more exposures, preceded and followed by an exposure of a Th-Ar comparison lamp. During this observing run, the relative humidity was quite high, particularly on the night of October 13, which led to a problem of condensation on the window of the CCD detector system. The spectral region most affected by this problem is the echelle order containing Hα.

Two sets of observations were obtained on 1995 November 28 and 29 with the University of Hawaii 2.2 m telescope using the f/34 coudé spectrograph with a 900 groove mm^{-1} grating blazed at 4400 Å, yielding a resolution of 0.10 Å pixel^{-1}. The slit was 1″ (350 μm) wide, projecting to 2 pixels on an Orbit 2048 × 2048 CCD. Both internal-lamp and dome flats were obtained each night as well as a series of bias frames. Each exposure of LS I+65 010 was of 20 minutes duration. Spectrophotometric standards were observed throughout the night, and Th-Ar comparison arc lamps were obtained each night for wavelength calibration.

Two additional sets were acquired in 2001, one on January 22 and one on October 13, also at the 2.1m of the OAN/SPM. The observations of January 22 were made using the CCD Thompson 2048×2048 detector. The observations of October 13 were made with the CCD SITe3. In Table 2 we list the mean values of the heliocentric Julian date, the orbital phases according to Crampton et al. (1985), the type of observation, the number of individual spectra for each set, the S/N near the He I 5875 Å line, and the useful wavelength range covered. In this table we have listed the orbital phases according to both the circular and the eccentric orbit solutions of Crampton et al (1985). However, in the remainder of this paper we will adopt the circular solution since it is more consistent with our observations (see Section 3.3). It is very important to note that according to the Crampton et al. circular orbit ephemeris, phase $\phi = 0$ corresponds to the phase at which the B-star is *receeding* fastest from the observer. Thus, the collapsed object is closest to the observer (i.e., "in front" of the B-star) at phase ~ 0.25 and "behind" the B-star at phase ~ 0.75. From Table 2 we can see that there is one set of observations (2001 Janunary) during which the collapsed companion was nearly "behind" the B-star. According to the eccentric orbit solution, ϕ=0 occurs at periastron passage.

Most of the data reduction was performed with IRAF, using the standard reduction procedures. The extraction and correction for the background of the echelle orders of the 2001 October data, however, was made using IDL. The images were corrected with the mean of the bias frames, and the 1993 and 1995 data sets were also corrected with the averaged and normalized flat field frames. The 2001 data were not corrected for flat fields because excessive noise would have been introduced by the flat fields. The orders of the echelle data were extracted and corrected for the background.

The wavelength calibration was performed using the comparison lamps (He-Ar) that were obtained nearest in time to the observation. The rms of the polynomial fits to the echelle dispersion functions were in all cases $\leq$ 0.05 Å. A shift in the zero point of the wavelength scale was applied to each set of spectra to place the principal component of the Na I 5889.95 Å line at its laboratory wavelength. The velocity shifts needed to accomplish this are listed in column 9 of Table 2. Also listed in this table, in the last column, is the value of ΔV_{helio}, the correction for the motion of the Earth with respect to the Sun, calculated with the *RVCORR* routine in IRAF. The difference between the values in these two columns (i.e., col.10−col.9), gives the correction that needs to be applied due to the motion of the Earth, to get the heliocentric velocity. The average value of this correction for the 7 data sets is −15 km s^{-1}. The conversion to velocities with respect to the LSR require an additional shift by + 7.2 km s^{-1}. The velocities listed in the tables are all measured with respect to the laboratory rest wavelengths as are references to velocities in the text, except when specifically noted otherwise.

The internal precision of the wavelength calibration was checked by comparing from spectrum to spectrum the following: 1) the wavelengths of the comparison lamp lines; 2) the wavelengths of the [OI] sky lines at 5577.335, 6300.304 and 6363.776 Å when observable; and 3) the wavelength of the diffuse interstellar bands (DIBs, see Herbig 1995), particularly the one at λ5849.65. We find that the accuracy of the wavelength calibration within each data set, for the same line measured on the same echelle order, is 3−6 km s^{-1}. The accuracy is largest in the red orders, and in the central portions of each order; it is lower in the blue orders and on the edges of each order because these portions of the echelle spectrogram have a smaller signal, and the extraction of the spectral orders is less accurate. In these regions of the spectra, the uncertainties are close to 20 km s^{-1} (∼one resolution element). Because of the large change in the response of the instrument between the center of the order and the edges, it was also found that the line profiles of photospheric lines that lie near the edges of the orders can change, from one order to the other overlapping order, in the same spectrum. Hence, we concentrate our attention only on lines that lie close to the center of the order. From the Na I line measurements we find that the internal precision of the RV measurements near He I 5875 Å is ±3 km s^{-1} for the echelle data and ±1 km s^{-1} for the coudé 1995 data.

One of the most serious problems with the echelle data is the rectification of the orders. This problem was more severe in the 2001 data than in the 1993 data. The instrumental response of each order of the 1993 data was removed by fitting a Legendre polynomial (usually of third order) to each order, for each spectrum, and dividing the data by this polynomial. In the majority of the spectral orders, this produced a flat normalized spectrum. This is not the case for the order containing the line of Hα where, due to the humidity problems, a satisfactory fit to the entire order was not achieved, so that the fit was made to the central portions of the order only. The data of 2001 were rectified using cubic spline functions, in some cases of orders as high as 15, and even then, the edges of the echelle order could not be fit in a satisfactory manner. We estimate that the uncertainty in the equivalent width measurements in the red, due to the rectification of the orders, is ∼5% near the center of the orders, and 10% near the edges. These estimates were obtained by repeatedly measuring W_λ's of the same lines in the same echelle order which, however was rectified with different functions (cubic splines and Chebychev) of orders ranging from 7 to 15, and averaging the resulting equivalent width measuremets of lines within the spectral order.

The signal-to-noise ratio (S/N) for the individual 1993 spectra ranges from ∼ 5 in the blue to ∼ 30 in the red, for the 1993 October 9 and 10 data, while for the October 13 data, the S/N is somewhat lower. For the 1995 data, S/N ∼ 35. The data of 2001 January have S/N ∼ 15 at 3850 Å, increasing with wavelength up to values of 120 in the red on some of the individual spectra. The data of 2001 October have S/N∼ 10 at 4400 Å and ∼80 in the red. Data in the blue were smoothed using Gaussian (σ=2) or boxcar smoothing functions before the measurements were made.

The line profiles were measured using the deblending routine in IRAF, fitting one, two, or three Gaussians to the data. In general, one Gaussian produces a very poor fit to the strong stellar line profiles because they are not symmetrical. Lines such as He I 5875 Å were fit well with two Gaussian functions which we will denote as the "blue" and the "red" Gaussian, (Vel^B and Vel^R, respectively) according to their location on the line profile. In general, the "red" Gaussian corresponds to the line core (i.e., the strongest portion of the line), while the "blue" Gaussian refers to the line wing on the short-wavelength side of the profile. We also measured the radial velocities using a single Gaussian fit (Vel^{One}), in order to be able to compare our velocities with those obtained by other authors.

Tables 3-5 list, in column 1, the identifying number of the spectrum, in column 2 its S/N value near He I 5875 Å, in column 3, the HJD (-2449000 for

1993; -2450000 for 1995 and -2451900 for 2001), and the orbital phase in column 4. In column 5, we list a phase that was computed using the 2.78 hour X-ray flaring period and the first value of the HJD in the corresponding table as the initial epoch; in Columns 6-7, we list the velocities of the two-Gaussian fits to He I 5875 Å, and, in columns 9-10, the corresponding equivalent widths (in Å); in column 8, we list the velocity obtained by measuring the centroid of the line with a single Gaussian fit. Finally, in column 11, we list the measured velocity of the Na I 5889.95 Å principal ISM component. Absence of data in these tables is in most cases due to the presence of a cosmic ray hit on the feature. In Table 6 we summarize the results of Tables 3-5 and list the average and standard deviations of the measured parameters.

3. RESULTS

3.1. *Spectrum and Interstellar Medium Components*

Figure 1 illustrates the blue portion of the 2001 Jan. spectrum of LS I+65 010. As in the spectra obtained by Crampton et al. (1985) and Reig et al. (1996), there is no evidence for He II 4686 Å line emission. The only emission line present is Hα. The other lines of the H-Balmer series are all in absorption, as are lines from He I, C III, Si III, O II among other ions. Reig et al. (1996) used the ratio of SiIII λ4552/HeI λ4387 to support their supergiant luminosity classification. For a Ia supergiant, this ratio ∼1, decreasing systematically for less luminous stars. From our data of 2001 we obtain SiIII λ4552/HeI λ4387∼0.90 (Jan.) and ∼0.80 (Oct.). It is interesting to note that Crampton et al.'s average values for these lines yields SiIII λ4552/HeI λ4387∼0.70. Hence, we find that this (classical) luminosity indicator is somewhat smaller than unity, but may be variable in LS I+65 010.

A new feature that is observable in the 1995 coudé data set is the presence of 3 resolved ISM components in the Na I D lines, as illustrated in Figure 2, where both atomic transitions are plotted on a velocity scale. The two high velocity components are labeled *a* and *b*. The third (principal) component is too broad to be attributed to a single ISM velocity, so we have assumed that it consists of at least two unresolved components, labeled (*c* and *d*). The four components were de-blended simultaneusly using the IRAF Gaussian fitting routines, and the radial velocities and equivalent widths of these features are listed in Table 7. The resulting velocities of these components, are v_{helio} -70, -48, -24, and -8 ± 3 km s^{-1}. Referred to the Local Standard of Rest these velocities are 7 km s^{-1} more positive. The echelle data do not have sufficient spectral resolution to allow the three individual components a,b, and c+d to be separated as clearly as in the Coudé data, and thus, the two high-velocity components are blended together, appearing as an extension towards shorter wavelengths of the principal (c+d) component. A similar profile is also present in the Ca II 3934 Åline.

If we assume that the Na I D lines are optically thin, we can estimate the column densities for each of the four velocity components, using (Spitzer 1978):

$$N(cm^{-2}) = 1.13 \times 10^{17} \frac{W_\lambda(m\AA)}{f\lambda^2(\AA)}, \qquad (1)$$

where *f* is the oscillator strength. This assumption is valid if each observed absorption consists of a blend of un-damped individual lines. The results are listed in Table 7. Note that the resulting column densities for the *c, d* components of Na I λ5895 are nearly twice the values derived from the Na I λ5889 line, showing that these components cannot be treated as a blend of un-damped lines, as expected from the fact that the absorptions reach zero intensity. Hence, the derived column densities for these components may be regarded only as lower limits. The approximation is more appropriate for each of the two high velocity components (*a* and *b*), for which we adopt the value $N_{col} = 1.4 \pm 0.3 \times 10^{12}$ cm^{-2}.

A sample of radial velocities of the interstellar lines in the northern Milky Way, as a function of Galactic longitude, is given by Münch (1957). At longitude *l* between 120° and 130° (LS I+65 010 lies at $(l,b)_{1950}$=(125°.7,+2°.6)), he reports a principal component at $v_{helio} \sim -4$ km s^{-1}, and a secondary components at $v_{helio} \sim -20$ km s^{-1}. Within the uncertainties, these velocities agree with the velocities we find for components *c* and *d*. The *d* component arises primarily in gas that is located in the Orion arm, within 0.5 kpc from the Solar neighborhood, while the *c* component arises in the Perseus spiral arm, which is at ∼2.5 kpc. The velocities are consistent with what is expected from the Galactic rotation curve. Our measured equivalent widths, however, are significantly (∼30%) smaller than those measured by Münch for the Orion arm regions, while our values for the Perseus arm equivalent widths lie within the range given by Münch.

Münch does not report the presence of higher velocity components at longitudes near that of LS I+65 010. In addition, due to the shape of the Galactic rotation curve (Clemens, 1985), such large negative velocities are excluded, even for regions that are at greater distances from the Sun. Hence, we conclude that components *a* and *b* are most likely associated with interstellar material in the vicinity of LS I+65 010, and which is expanding away from this system. We do not detect any variability in the ISM components between our data sets.

3.2. *W_λ-RV correlation and the systemic velocity*

The equivalent width and the centroid of the unblended photospheric absorption lines with good S/N were measured on each spectrum of each epoch. The best data correspond to the 2001 January data set, and are listed in Table 8. Column 1 gives the laboratory wavelength of the absorption; column 2, the average velocity (in km s^{-1}, with respect to its laboratory wavelength); column 3, the Gaussian FWHM (in km s^{-1}); column 4, the equivalent width (in Å); column 5 the value of log(gf), where g is the statistical weight and f the oscillator strength of the transition; and column 6, comments. All values of log(gf) were taken from the data base available electronically at the National Institute of Standards and Technology (*http://physics.nist.gov*). For the 2001 October data it was possible to measure reliably only about half of the lines (listed in Table 9).

The data in Tables 8 and 9 are plotted in Figure 3 and suggest the presence of a correlation between equivalent widths and radial velocity. In this figure we plot the data obtained on 2001 January (dark symbols) and October (light symbols). The H and He lines (triangles and crosses, respectively) observed in 2001 January were used to test the reality of the trend. A Spearman's rank correlation coefficient between RV and the EW is r=0.79 with a two-sided significance of 0.001 of its deviation from zero (small value means a significant correlation).

Also, the systematic velocity shift of 15 km s^{-1} is evident between the data of January (dark symbols) and October (light symbols), which coincides with the reported semi-amplitude of the radial velocity curve (Crampton et al. 1985; see below). The RVs of the weaker lines are clustered near -20 km s^{-1}, and the strongest lines have RVs ~-50 km s^{-1}.

Aab & Bychkova (1983) and Crampton et al. (1985) noted the presence in LS I+65 010 of a correlation between radial velocity and the excitation of the atomic transition responsible for the line, and this is, generally speaking, the same effect we are observing in our data. Hutchings (1976, and reference therein) was the first to study this correlation in a large sample of stars, and more recent analyses have been made by Massa et al. (1992) and Kudritzky (1992). The explanation for this effect is that the atmospheres of hot stars are not in hydrostatic equilibrium, except perhaps, for the deepest-lying layers. Thus, there is a velocity gradient in the line-forming regions. Lines that have large opacities, and are therefore observed to arise in exterior atmospheric layers, are shifted to shorter wavelengths than lines that can be observed arising from deeper layers (i.e., the optically thinner lines). In Figure 4 we plot the same H and He I data shown in Figure 3 for the 2001 January data but use the value of log(gf) in the ordinate, instead of equivalent width. A very clear correlation is observed, confirming the dependence of the measured velocity on the transition probability of the line. Given these effects, it is clear that the the best approximation to the actual radial velocity of the B-star is the velocity given by the lines with the smaller log (gf). For the 2001 January data, this value is -20 ± 5 km s^{-1}, with respect to the laboratory reference frame, so $v_{helio}=-35$ km s^{-1}.

If the photosphere is stable, and its expansion velocity gradient remains constant throughtout the orbital cycle, then the orbital motion may be well described by the strong absorption lines. If this is not the case, it is necessary to determine the orbital parameters exclusively from the weaker lines.

Adopting the Crampton et al. (1985) orbital solution, our 2001 January data are very close to a conjunction, and thus the measured radial velocity should be very close to the velocity of the system; i.e., the velocity at ϕ=0.71 is -4 km s^{-1} with respect to the systemic velocity. Therefore, the velocity of the LS I+65 010 system is $v_{helio}=-31\pm5$ km s^{-1}. This velocity coincides with the radial velocity of the cluster NGC 281 (at l=126°) and which lies at a distance of 2.9 kpc (Hron 1987). Hence, assuming that the systemic radial velocity is due entirely to the effect of galactic rotation, we conclude that LS I+65 010 is likely to be located in the Perseus arm within $\sim$ 3 kpc from the Sun. However, it is possible for the system to have a peculiar velocity, given the fact that the neutron star is the result of a supernova explosion. Hence, the observed radial velocity may have a contribution from the peculiar velocity obtained during the SN event.

3.3. *Radial Velocity Variations*

In this section we concentrate the analysis on He I 5875 Å for the following reasons: 1) the 7 data sets contain this line, and thus it is the only line for which a relatively broad orbital phase coverage is available; 2) its proximity to the ISM Na I D lines and the DIB at 5849 Å allows an accurate check on the wavelength scale; 3) it lies near the center of the echelle order, and this order has a good S/N.

In Fig. 5 we reproduce the Crampton et al. (1985) RV data (open triangles), plotted as a function of the orbital phase (P=11.591; circular orbit solution), upon which we superpose the mean RVs of He I λ5875 (filled squares) measured with a single Gaussian fit (Vel^{One}), taken from Table 6. Our data, though scant, coincide very well with the Crampton et al. RV data. Note, however, that the velocities of Table 6 are measured with respect to the laboratory wavelength. Although not specified in the Crampton et al. (1985) paper, their data are most likely heliocentric velocities. This means that although the shape of the RV curve determined by our scant data points coincides well with the Crampton et al. RV curve, if heliocentric velocities were plotted, our RV data would be displaced by ~-15 km s^{-1}. This is not surprising, since the Crampton et al. RV curve is based on the average velocity of a wide range of absorption lines (including lines with smaller RVs), while our data points refer only to He I 5875 Å which is one of the most blue-shifted lines in the optical spectral range. Figure 5 also includes the data published by Reig et al (1996) for the He I 6678 line. These data follow the Crampton et al. RV curve except at phases ϕ=0.4 - 0.7, when a large excursion to much more negative velocities is observed.

We also plotted our data using the eccentric orbit ephemeris (P=11.588 days) given by Crampton et al., and we find that our data are shifted by ~0.1 in phase, with respect to the mean RV curve of Crampton et al., plotted with this same period. Hence, the 11.588 day period may now be discarded. A more complete phase phase coverage is needed in order to further improve on the accuracy of the 11.591-day period.

We indicate in Fig. 5 the approximate phase intervals during which the RXTE X-ray counts (from Corbet et al. 1999) are maximum (0.25-0.75) and minimum (0.75-0.25). Note that these phase intervals are centered on elongations (i.e., maximum approaching and receding velocities of the stars), rather than on conjunctions, so that the X-ray minimum cannot be attributed to an eclipse of the X-ray source. As pointed out by Corbet et al. (1999), it is difficult to understand why the RV curve and the X-ray variations on orbital timescales present this inconsistency.

An additional problem arises when we compare the RV values of the He I λ5875 Å line core (Vel^{R}) with the values of Vel^{One} as a function of orbital phase (Fig. 6). Vel^{One} is the radial velocity that is obtained from the centroid of the whole line profile, while Vel^{R} is the radial velocity of the "red" portion of the line profile (which is actually the strong line core), when it is fit with two Gaussians. If the line profile were to remain constant throughout the orbital cycle, both of these velocities whould describe the same radial velocity curve, except for a constant velocity shift between them. However, this is does not occur in LS I+65 010: Vel^{R} and Vel^{One} have similar values near $\phi = 0.$ (X-ray minimum), but very different values near $\phi = 0.5$ (X-ray maximum). This discrepancy is due to the presence of a much stronger blue wing in the absorption feature at $\phi = 0.36$ (see Section 3.4), which leads to a displacement of the line centroid (Vel^{One}) to more negative velocities. The variation of the He I 5875 Å blue wing equivalent width is displayed in Figure 7, where an increase around 0.36-0.45 is observed. Because of the limited number of orbital phases covered by our data, and because we do not have repeat observations at the same phases, we are unable to conclude that the line-profile variations are phase-locked, and therefore actually distort the RV curve. However, Barsiv et al. (2001) observe a distortion of the RV curve obtained from the Hγ line in the optical counterpart of the Vela X-1 that can be traced to line profile variability. That is, they also detect the appearance of an extended blue wing on the photospheric absorption. It is possible also that the RV measurements of He I 6678 Å obtained by Reig et al. (1996), and plotted in Figure 5, may be affected by the appearance of a blue wing.

3.4. *Line profile variability*

We illustrate the type of line profile variability that occurs in He I 5875 Å from night to night in Figures 8-9. In Figure 8 we compare the line profile at phase 0.71, with the profiles at phases 0.89 and 0.36. The line profile observed at orbital phase $\phi = 0.71$ is the strongest and most symmetrical, among our data sets. The line profile observed at $\phi = 0.89$ displays weaker absorption, and presents indications of the presence of emission superposed at least on its red wing. At this phase, the neutron star is near the elongation at which it has the maximum approaching velocity, and any emission arising in its vicinity would be expected to be blue-shifted. It is possible that the reduced strength of the photospheric absorption is a result of the line being filled-in by such emission. The profile at $\phi = 0.36$ also presents indications of emission on the red wing, but, in addition, the blue wing has excess absorption.

The Hα line is available in only 5 of the 7 data sets, but due to severe fringing problems in the 2001 Jan data within this spectral region, we are not able to reliably use this Hα line profile. A montage of the line profiles is presented in Figure 10. At orbital phase 0.07 Hα presents an emission-line profile upon which a prominent absorption feature is superimposed, shortward of the line center. At phase 0.15, the absorption is weaker, and by phase 0.41 it has been replaced by emission. A similar change in this line on the same timescale is reported to have occurred in 1984 by Minarini et al. (1994). The average (for each night) equivalent width of the emission component does not change appreciably, having a value of $W_\lambda = 1.2 \pm 0.1$ Å, very similar to the value obtained by Reig et al.(1996). Variations mainly on the blue wing of the line profile of Hα have also been reported by Liu & Hang (1999), who favor contamination by emission, due to the presence of an ionized bubble surrounding the neutron star. This ionized region would be expected to partake in the orbital motion of the neutron star. Hence, the extra emission would tend to "fill in" the blue wing of the photospheric absorption lines only when it is approaching the observer. According to the radial velocity curve of Crampton et al., this is at ϕ∼0.80-1.20. In Figure 10 we do observe a weak emission centered at −270 km s^{-1} at ϕ=0.07, while at ϕ=0.41, there is some indication of excess emission at +200 km s^{-1}. However, the line profiles are too noisy for these excess emissions to be quantified with precision. At phase 0.41 there is no trace of the photospheric absorption, implying that it is completely filled in by the emission. Thus, the Hα line profiles do provide support for the hypothesis of an H II region surrounding the neutron star. However, if this were the only source for the emission, a much stronger red-shifted emission whould be present at phase 0.41 than is observed. Hence, we conclude that there is a persistent component to the Hα emission centered at ∼+80 km s^{-1} that does not follow the orbital motion of the neutron star, and that most likely arises in the wind of the B1-star.

3.5. *Variability on the 2.78 hour X-ray flaring period*

We searched for variability with $P = 2.78$ hours in all the radial velocity and equivalent width measurements of He I. We were unable to detect any convincing modulation in any of the data sets, although variations of up to 40 km s^{-1} in the "blue" (Vel^B) 2-Gaussian fit to the data were detected within a single night. In Figures 11-12 we plot the velocity of the "red" Gaussian (that corresponds to the core of the line) as a function of phase calculated for the 2.78 hour period, for the nights 1995 Nov. 28, 29, (Fig.11) and 2001 Jan 22, Oct 13 (Fig. 12). The uncertainties in these measurements are ∼10 km s^{-1}. The 2001 data (orbital phases 0.71 and 0.89) are practically constant throughout the night. There is a moderate (∼15 km s^{-1}) amount of variability in the 1995 Nov. data (orbital phases 0.36 and 0.45), but with little evidence indicating that this variability follows the 2.78 hour period. The degree of variability is largest for the blue wing of He I 5875 Å in the 1995 data sets (Figure 13), although a possible modulation on the 2.78 hour period that is observed on the Nov. 29 data depends on 3 data points, and thus can only be considered as marginal evidence in favor of the presence of this modulation.

4. CONCLUSIONS

We present the results obtained from optical spectral observations of the X-ray binary system 2S0114 +650=LS I+65 010. The radial velocity curve obtained from our data are inconsistent with the eccentric orbit solution given by Crampton et al. (1986), and thus we favor the P=11.591 days solution, which assumes a circular orbit.

The correlation between the equivalent width of the lines and their radial velocity is used to estimate the systemic radial velocity. Strong lines have the largest negative velocities because they form further out in the atmosphere, where expansion velocities are greater than in the inner atmospheric layers. Hence, the weaker lines provide a more accurate estimate of the actual radial velocity of the B1-star, which we find to be V$_{helio}$=−31 km s^{-1}. Assuming that the radial velocity is due to Galactic rotation leads us to conclude that LS I+65 010 is at ∼ 3 kpc. This distance is near the lower limit of the distance of 7±3.5 kpc derived by Reig et al. (1996). Caution is necessary, however, because the SN event that occurred in this system might have given it a peculiar velocity with respect to its expected velocity due to the Galactic rotation curve. The spectral luminosity indicator SiIII λ4552/He I λ4387 ∼0.9 in our data, while in the Crampton et al. data it is 0.7, both values consistent with a high luminosity for the B1-star. If it is a supergiant (λ4552/He I λ4387∼1), then a larger distance is expected.

Significant line profile variability is detected from night to night. The He Iλ5875 photospheric line presents an additional, blue-shifted absorption component at orbital phases 0.36 and 0.45, thus enhancing the generally present asymmetry of this line. The extension of this blue wing is −400 km s^{-1}, far in excess of the broadening that could be attributed to the 100 km s^{-1} rotational velocity of the B1-star, and indicates that these wings form in portions of the photosphere that are not only expanding, but where the expansion may depend on the orbital phase. A similar blue-shifted component to this absorption line appears in the spectra of HD 7751, the optical counterpart of Vela X-1 (Barziv et al. 2001), at orbital phases 0.45-0.67, which in this case correspond to phases when the neutron star in "in front" of the B-star primary. In LS I+65 010, phases 0.36-0.45 are closer to an elongation, although the neutron star is still on the near side (with respect to the observer) of the B1-star. We note that the X-ray maximum occurs at phase 0.5 in LS I+65 010, so there may be a connection between the appearance of the extra blue-shifted absorption and the enhanced X-ray emission. Our data, however, are insufficient to be able to conclude that the observed variability is phase-locked, although this conclusion was reached by Barziv et al. (2001) for the case of Vela X-1.

Significant variability on an hourly timescale was detected only for two of our data sets (1995; orbital phases 0.36 and 0.45). However, we are unable to conclude that this variability is periodic, on the 2.78 X-ray flaring period. It is clear, however, that the strongest variability occurs on the blue portions of the line profiles, consistent with the notion that the photospheric layers at the base of the wind are not undergoing a steady expansion, at least at these orbital phases where the variability is detected. Hence, the effect of the neutron star on the companion's atmosphere may not be negligible.

Two high velocity components ($V_{helio} = -70$ and -49 km s^{-1}) are detected in the Na I D lines that may be associated with a circumstellar H II region surrounding LS I+65 010. This region would have to have formed after the SN explosion, and thus suggests possible shell ejections from the B-star. However, we cannot at this stage discard intervening high velocity clouds as the source of these absorptions.

The behavior of the RXTE X-ray light curve obtained by Corbet et al. (1999) cannot be explained if the Crampton et al. RV curve represents the true orbital motion of the B star. We have tested various scenarios, such as the presence of a disc, an eccentric orbit and a non-spherically symmetric wind, and all of these scenarios demand that X-ray minimum occur when the neutron star is behind the B1-star (phase 0.75); or the presence of two maxima, assuming the orbit of the neutron star intersects a high density disk surrounding the B1-star. None of these correspond to the observations. The only contribution we can make towards trying to solve this dilemma is the finding that X-ray maximum appears to be correlated with the presence of a more extended blue wing in some of the photospheric absorption lines. Comparing the He I 5875 line profiles of LS I+65 010 with the same line profiles in Vela X-1 (Fig. 17 of Barziv et al. 2001), and assuming that similar processes occur in both binary systems, it is tempting to speculate that the Crampton et al. (1985) radial velocity curve may be distorted in the phase range ~0.3-0.5, such that at $\phi \sim 0.5$ the neutron star is actually "in front" of the B1-star, rather than at an elogation. Clearly, however, an understanding is necessary of the processes involved in producing the line-profile variability before this speculation can be taken a step further. In addition, it would be most desirable to obtain radial velocity measurements throughout the orbital cycle of 2S0114+650 from the upper Balmer lines and weak metal lines, all of which are much less affected by the non-stationary nature of the outer expanding photosphere.

We are grateful to an anonymous referee for the meticulous revision of the submitted versions, resulting in a much improved paper. We thank John Dvorak, Salvador Monrroy, and J. Velazco for their assistance with the spectroscopic observations. GK thanks M. Peimbert and D. Massa for enlightening discussions. We thank Elfego Ruiz and Daniel Peña for technical advice, and the University of Hawaii for granting observing time. Extensive use was made of the atomic lines data bases available through the National Institute of Standards and Technology (NIST). Part of this work was performed under the auspices of the U.S. Department of Energy, National Nuclear Security Administration by the University of California, Lawrence Livermore National Laboratory under contract No. W-7405-Eng-48, and and grants from CONACYT and from UNAM/DGAPA.

REFERENCES

Aab,O.E., Bychkova,L.V., Kopylov, I.M. 1983, Sov. Astron. Lett. 9, 285.

Aab, O.E., Bychkova, L.V. 1983, Sov. Astron. Lett. 9, 313.

Barziv, O., Kaper, L., Van Kerkwijk,M.H., Telting, J.H., Van Paradijs, J. 2001, A&A 377, 925.

Bell, S.A., Hilditch, R.W., Pollacco,D.L. 1993, MNRAS 251, 66p

Clemens, D.P., 1985 ApJ 295, 422

Corbet, Robin H. D., Finley, J.P., Peele, A.G. 1999, ApJ 511, 876.

Crampton, D., Hutchings, J.B., Cowley, A.P. 1985, ApJ 299, 834

Diego, F. & Echevarria, J. 1994, Reporte Técnico, Instituto de Astronomía, UNAM.

Dower, R., Kelley, R., Margon, B., Bradt,H. 1977, IAUC 3144.

Finley, J.P., Belloni, T., Cassinelli, J.P. 1992, ApJ 262, L25

Finley, J.P., Taylor, M., Belloni, T. 1994, ApJ 429, 356.

Gotthelf, E.V., Gavriil, F.P., Kaspi, V.M., Vasisht, G., Chakrabarty, D., 2002, ApJ 564, 31.
Hall, T.A., Finley, J.P., Corbet, R.H.D., Thomas, R.C. 2000, A&A 536, 450.
Herbig, G. 1995, ARA&A 33, 19.
Hron, J. 1987, A&A 176, 34.
Hutchings, J.B. 1976, ApJ 203, 438.
Koenigsberger, G., Swank, J.H., Szymkowiak, A.E., White, N.E. 1983, ApJ 268, 782
Kholopov, et al. 1989, IBVS 3323.
Kudritzky, R.P.1992, A&A 266, 395.
Kumar, P., Ao, C.O., Quataert, E.J. 1995, ApJ 449, 294
Li, X.-D., van den Heuvel, E.P.J. 1999, ApJ 513, L45
Liu, Q.-Z., Hang, H.-R. 1999, A&A 350, 855.
Marsden, D., Rothchild, R.E., Lingenfelter, R.E. 1999, ApJ 520, 107.
Massa, D. 1992, A&A 264, 169
Minarini, R., Teodorani, M, Bertolini, C., Guarnieri, A., Piccioni, A.: 1994, in *The Evolution of X-ray Binaries*, S.S. Hold and C.S. Day eds, AIP Conf. Proc. p. 275.
Margon, B. 1977, IAU Circ. 3144.
Margon, B. 1980, Proceedings 9th Texas Symposium on Relativistic Astrophysics (eds.) J. Ehlers, J.J.Perry, M. Walker, Ann. N.Y. Acad. Sci. 336,550.
Münch, G. 1957, ApJ 125, 42.
Reig, P., Chakrabarty, D., Coe, M.J., Fabregat, J., Negueruela, I., Prince, T.A., Roche, P., Steele, I.A. 1996, AA 311, 879.
Taylor, M., Finley, J.P., Kurt, C., Koenigsberger, G. 1995, AJ 109, 396.
Vogt,S.S., Penrod, G.D. 1983, ApJ 275, 661.
Spitzer, L. 1978, *Physical processes in the interstellar medium*, New York Wiley-Interscience.
Witte,M.G., Savonije G.,J. 1999, ApJ 350, 129
Yamauchi, S., Asaoka, I., Kawada, M., Koyama, K., Tawara, Y. 1990, Publ. Astron. Soc. Japan 42, 153.

Anabel Arrieta,Leonid Georgiev, Gloria Koenigsberger, Michael Richer: Instituto de Astronomía, UNAM, Apdo. Postal 70-264, México D.F. 04510 (anabel,georgiev,gloria,richer@astroscu.unam.mx)
Gloria Koenigsberger:Centro de Ciencias Físicas, UNAM, Apdo. Postal 48-3, Cuernavaca,Mor, 62251, México
Gabriela Canalizo:Institute of Geophysics and Planetary Sciences, Lawrence Livermore National Laboratory, 7000 East Avenue, L-413, Livermore, CA 94550

TABLE 1

PARAMETERS OF LS I+65 010 = 2S 0114+650

Parameter	Value	Notes and references
Spectral type	B1 Ia	5
T_{eff}	24000 ± 3000	5
$R/R_\odot$	37 ± 15	5
$M/M_\odot$	15 ± 5	5
M_V	-7.0 ± 1.0	5
Distance (kpc)	7.0 ± 3.5	5
	2.5	2
vsini (km/s)	96 ± 20; 46	5,2; 7
E(B-V)	1.24 ± 0.02	5
log g	2.5 ± 0.2	5
BC	-2.3 ± 0.3	5
M_{bol}	-9.3 ± 1.0	5
Orbital period (d)	11.588 ± 0.003	e=0.16; 2
	11.591 ± 0.003	e=0; 2
Initial Epoch T_o	2444134.9 ± 0.7	e=0.16; 2
	2444134.3 ± 0.2	e=0; 2
K (km s^{-1})	17 ± 1	2
L_x(1.5-10 kev)	1.3×10^{35}	d=2.5 kpc; 2
	1.1×10^{36}	6
P_{pulse} (secs)	893.8 ?	1
	850	3
$P_{X-flares}$ (hrs)	2.78	4
	2.73	6
$T_{o,X-flares}$	2446433.632 ± 0.06	4

References for Table 1: 1) Koenigsberger et al. 1983; 2) Crampton et al. 1985; 3) Yamauchi et al. 1990; 4) Finley et al. 1992; 5) Reig, et al. 1996; 6) Hall et al. 2000; 7) Aab et al. 1983. T_o corresponds to periastron passage in the eccentric orbit and maximum positive velocity in circular orbit.

TABLE 2

SUMMARY OF THE OBSERVATIONS

Year	mean HJD -2400000	ϕ^{circ}	ϕ^{ecc}	Type	Num.	S/N at λ5875	λ-range Å	zero-point shift km s^{-1}	ΔV$_{helio}$ km s^{-1}
1993	49269.943	0.07	0.13	SPM echelle	5	26-33	4300-6650	+22	9.5
1993	49270.834	0.15	0.21	SPM echelle	10	16-37	4300-6650	+22	9.1
1993	49273.894	0.41	0.47	SPM echelle	14	17-27	4420-6600	+20	8.4
1995	50049.882	0.36	0.44	UH coudé	13	30-45	5815-5956	+10	-5.9
1995	50050.884	0.45	0.53	UH coudé	10	20-47	5815-5956	+ 8	-6.1
2001	51931.682	0.71	0.83	SPM echelle	11	50-120	3700-7500	- 1	-18.0
2001	52095.858	0.87	0.00	SPM echelle	14	40-80	4350-6850	+26	8.4

TABLE 3

ECHELLE 1993 OBSERVATIONS OF HE I 5875

ID (1)	S/N (2)	HJD (3)	ϕ^{cir} (4)	ϕ^{flare} (5)	Vel^{B} (6)	Vel^{R} (7)	Vel^{One} (8)	W_{λ}^{B} (9)	W_{λ}^{R} (10)	NaI (11)
3	20.	49269.860	0.065	0.000	-260	-43	-46	0.16	1.00	0
7	25.	49269.918	0.070	0.501	-200	-44	-52	0.25	0.92	-3
9	27.	49269.947	0.072	0.751	-197	-41	-46	0.15	0.89	0
11	32.	49270.000	0.077	0.209	-209	-45	-50	0.11	0.93	-1
13	25.	49270.026	0.079	0.434	-197	-43	-47	0.14	0.81	-2
6	32.	49270.712	0.138	0.358	-246	-39	-40	0.10	0.91	1
8	26.	49270.740	0.141	0.599	-254	-38	-40	0.12	0.91	0
10	33.	49270.765	0.143	0.815	—	—	—	–	–	-1
12	32.	49270.792	0.145	0.048	-234	-38	-43	0.20	0.90	-2
14	30.	49270.818	0.147	0.273	-233	-38	-38	0.13	0.90	0
16	20.	49270.860	0.151	0.636	—	—	—	–	–	-4
18	26.	49270.885	0.153	0.852	-239	-39	-44	0.19	0.92	-3
22	26.	49270.932	0.157	0.257	-216	-37	-44	0.19	0.80	-4
23	26.	49270.943	0.158	0.352	-252	-41	-42	0.16	0.89	-5
24	20.	49270.957	0.159	0.473	-245	-41	-43	0.12	0.91	-3
6	17.	49273.774	0.402	0.800	-162	-28	-47	0.10	0.96	3
10	21.	49273.840	0.408	0.370	-178	-29	-49	0.27	0.74	0
11	23.	49273.851	0.409	0.465	-195	-38	-46	0.17	0.77	-3
13	15.	49273.874	0.411	0.663	—	—	—	–	–	-2
14	19.	49273.886	0.412	0.767	-171	-31	-53	0.25	0.79	-3
15	16.	49273.897	0.413	0.862	—	—	—	–	–	-3
16	14.	49273.907	0.414	0.948	-276	-50	-58	0.20	0.94	-5
18	22.	49273.936	0.416	0.199	-215	-36	-50	0.24	0.80	-3
19	19.	49273.947	0.417	0.294	—	—	—	–	–	–
20	14.	49273.958	0.418	0.389	—	—	—	–	–	-5
21	13.	49273.980	0.420	0.579	—	—	—	–	–	-5
22	15.	49273.991	0.421	0.674	-203	-36	-58	0.29	0.90	-5
23	18.	49274.003	0.422	0.777	-222	-51	-56	0.21	0.77	-5
24	13.	49274.015	0.423	0.881	—	—	-62:	–	–	-8

TABLE 4

COUDÉ 1995 OBSERVATIONS OF HE I 5875

ID (1)	S/N (2)	HJD (3)	ϕ^{cir} (4)	ϕ^{flare} (5)	Vel^{B} (6)	Vel^{R} (7)	Vel^{One} (8)	W_{λ}^{B} (9)	W_{λ}^{R} (10)	NaI (11)
21	31.	50049.802	0.353	0.000	-176.	-27.	-73.	0.60	0.56	1.
22	30.	50049.816	0.354	0.121	-195.	-31.	-65.	0.41	0.77	1.
23	33.	50049.828	0.355	0.224	-166.	-21.	-76.	0.61	0.56	0.
24	33.	50049.839	0.356	0.319	-166.	-23.	-71.	0.58	0.60	0.
25	35.	50049.851	0.357	0.423	-192.	-36.	-80.	0.55	0.62	-1.
26	36.	50049.863	0.358	0.526	-165.	-29.	-79.	0.60	0.54	0.
28	40.	50049.879	0.360	0.664	-173.	-25.	-73.	0.58	0.62	0.
29	43.	50049.894	0.361	0.794	-181.	-30.	-70.	0.38	0.64	1.
30	45.	50049.908	0.362	0.915	-186.	-29.	-79.	0.46	0.66	0.
31	44.	50049.923	0.363	1.044	-195.	-36.	-65.	0.30	0.69	0.
32	36.	50049.937	0.365	1.165	-204.	-27.	-68.	0.48	0.74	1.
33	34.	50049.954	0.366	1.311	-218.	-36.	-75.	0.35	0.69	1.
34	35.	50049.968	0.367	1.432	-190.	-25.	-67.	0.39	0.68	1.
97	47.	50050.780	0.437	8.438	-222.	-48.	-59.	0.28	0.77	0.
98	43.	50050.796	0.439	8.576	-221.	-50.	-64.	0.29	0.77	1.
99	40.	50050.810	0.440	8.697	-223.	-50.	-58.	0.22	0.79	0.
100	27.	50050.825	0.441	8.827	-220.	-48.	-66.	0.26	0.72	0.
101	23.	50050.841	0.443	8.965	-231.	-57.	-75.	0.30	0.85	0.
102	24.	50050.855	0.444	9.085	-240.	-56.	-84.	0.37	0.74	0.
103	35.	50050.870	0.445	9.215	···	-46.	-60.	0.22	0.73	0.
104	23.	50050.885	0.446	9.344	-233.	-46.	-55.	0.28	0.77	0.
106	37.	50050.915	0.449	9.603	-222.	-55.	-67.	0.26	0.75	0.

TABLE 5

ECHELLE 2001 OBSERVATIONS OF HE I 5875

ID	S/N	HJD	ϕ^{cir}	ϕ^{flare}	Vel^{B}	Vel^{R}	Vel^{One}	W_{λ}^{B}	W_{λ}^{R}	NaI
(1)	(2)	(3)	(4)	(5)	(6)	(7)	(8)	(9)	(10)	(11)
4020	80.	51931.616	0.705	0.004	-228.	-58.	-63.	0.12	1.14	-1.
4021	120.	51931.627	0.705	0.099	···	-62.	-65.	0.06	1.23	-1.
4023	79.	51931.641	0.707	0.220	-287.	-59.	-66.	0.10	1.17	-1.
4024	76.	51931.652	0.708	0.315	-342.	-58.	-62.	0.06	1.17	-1.
4025	100.	51931.664	0.709	0.419	-203.	-62.	-66.	0.08	1.15	0.
4026	85.	51931.676	0.710	0.522	-274.	-58.	-68.	0.18	1.24	1.
4028	87.	51931.690	0.711	0.643	-237.	-59.	-63.	0.08	1.18	0.
4030	53.	51931.713	0.713	0.842	-128.	-66.	-66.	0.05	1.14	-7.
4031	67.	51931.725	0.714	0.946	-270.	-63.	-63.	0.05	1.16	-2.
4032	95.	51931.736	0.715	0.041	-267.	-60.	-65.	0.07	1.17	2.
4033	80.	51931.748	0.716	0.144	-211.	-60.	-61.	0.07	1.16	3.
1066	80.	52095.776	0.867	0.621	-214.	-39.	-43.	0.04	0.68	0.
1067	75.	52095.787	0.868	0.716	-133.	-38.	-39.	0.05	0.71	2.
1069	67.	52095.804	0.870	0.863	-227.	-35.	-42.	0.04	0.67	1.
1070	64.	52095.815	0.871	0.958	-214.	-38.	-41.	0.05	0.68	1.
1071	80.	52095.826	0.872	0.053	···	···	···	···	···	-1.
1073	77.	52095.844	0.873	0.208	-233.	···	···	···	···	1.
1075	62.	52095.866	0.875	0.398	-167.	···	···	0.03	0.63	-5.
1077	50.	52095.881	0.876	0.528	-268.	-41.	-41.	0.01	0.68	3.
1078	77.	52095.892	0.877	0.623	-214.	-36.	-39.	0.01	0.68	2.
1079	72.	52095.903	0.878	0.718	···	···	···	···	···	5.
1081	50.	52095.918	0.879	0.847	···	···	···	···	···	5.
1083	65.	52095.940	0.881	0.037	-188.	-34.	-38.	0.06	0.70	4.

TABLE 6

SUMMARY OF THE PROPERTIES OF HE I λ5875

ID (1)	HJD (2)	ϕ^{cir} (3)	Vel^{B} (4)	Vel^{R} (5)	Vel^{One} (6)	W$_{\lambda}^{B}$ (7)	W$_{\lambda}^{R}$ (8)	NaI (9)
1993 Oct. 9	49269.943	0.07	-213 ± 27	-43 ± 1	-48 ± 3	0.16 ± 0.05	0.91 ± 0.07	-1 ± 1
1993 Oct. 10	49270.834	0.15	-240 ± 12	-39 ± 1	-42 ± 2	0.15 ± 0.04	0.89 ± 0.04	-2 ± 2
1993 Oct. 13	49273.894	0.41	-203 ± 36	-37 ± 9	-53 ± 6	0.22 ± 0.06	0.83 ± 0.08	-3 ± 3
1995 Nov. 28	50049.882	0.36	-185 ± 16	-29 ± 5	-72 ± 5	0.48 ± 0.11	0.64 ± 0.07	0.3 ± 0.7
1995 Nov. 29	50050.884	0.45	-226 ± 7	-51 ± 4	-65 ± 9	0.27 ± 0.04	0.77 ± 0.04	0 ± 0.3
2001 Jan. 22	51931.682	0.71	-230 ± 77	-60 ± 3	-64 ± 2	0.08 ± 0.03	1.17 ± 0.03	-1 ± 3
2001 Oct. 13	52095.858	0.87	-173 ± 63	-37 ± 2	-40 ± 2	0.04 ± 0.02	0.68 ± 0.02	2 ± 3

TABLE 7

NA I ISM COMPONENTS

	Na I λ5889.950				Na I λ5895.924			
	a	*b*	*c*	*d*	*a*	*b*	*c*	*d*
f_{ik}	0.647				0.322			
V (km s^{-1})	-55	-34	-9	$+8$	-55	-33	-8	$+7$
V_{helio} (km s^{-1})	-70	-49	-24	-7	-70	-69	-23	-8
W_λ (Å)	0.215	0.210	0.330	0.315	0.177	0.172	0.300	0.300
N_{col} (10^{12}cm^{-2})	1.08	1.06	>1.66	>1.59	1.77	1.74	>3.03	>3.03

TABLE 8

MEAN RADIAL VELOCITIES AND EQUIVALENT WIDTHS IN JANUARY 2001

Line ID (1)	RV km s^{-1} (2)	GFWHM km s^{-1} (3)	W_λ Å (4)	log(gf) (5)	Comments (6)
H I					
4101.74	-34	280	0.90	-1.108	
4340.47	-46	220	1.12	-0.796	
4861.33	- 55	230	1.20	-0.358	
6562.82	-117	160	0.60	0.144	abs. superposed on emission
HeI					
3926.53	-19	275	0.38	-1.647	seen only in mean
3964.73	-25	130	0.30	-1.295	
4009.27	-23	140	0.28	-1.473	
4026.28	-42	190	0.73	-0.701	blend 4026.19+4026.36
4143.76	-33	170	0.45	-1.196	
4387.93	-37	160	0.50	-0.883	blend w/ C III 4388.02
4471.58	-52	170	0.93	-0.278	blend 4471.48+4471.69
4713.26	-34	130	0.35	-1.230	blend 4713.15+4713.38
4921.93	-33	150	0.79	-0.435	
5015.68	-33	135	0.42	-0.820	
5047.74	-22	128	0.24	-1.601	blended w/ N II 5045
5875.80	-57	180	1.25	0.408	blend:5875.62+ 5875.97
6678.15	-46	150	1.18	0.329	

TABLE 9

CONT.

Line ID (1)	RV km s^{-1} (2)	GFWHM km s^{-1} (3)	W_λ Å (4)	log(gf) (5)	Comments (6)
C III					
4388.02	-46	160	0.51	-0.506	strong line
5695.92	-7	140	0.18	0.0170	
N II					
3995.00	-42	110	0.30	0.208	
5045.099	-32	170	0.18	-0.407	blended w/ He I
5676.02	-17	170	0.18	-0.367	
5679.56	-37	140	0.33	0.250	
O II					
4075.86	-40	130	0.20	0.693	
4319.63	-31	120	0.21	-0.380	blended w/ line above
4345.56	-30	120	0.21	-0.346	
4366.90	-43	140	0.22	-0.348	
4414.91	-29	160	0.25	0.172	blended w/ line below
4416.98	-32	80	0.12	-0.077	blended w/ line above
4590.97	-35	112	0.19	0.350	
4661.64	-28	130	0.24	0.278	
4699.21	-25	140	0.08	0.270	
Si III					
4552.62	-36	130	0.45	0.292	nice symmetrical line
4567.83	-40	120	0.38	0.070	
4574.76	-35	130	0.26	-0.406	
4819.74	-35	180	0.24	na	
5739.73	-20	170	0.35	-0.157	
Si IV					
4116.10	-25	110	0.16	-0.106	
Mg II					
4481.23	-51	160	0.23	0.730	blend 4481.13+4481.33+OII

TABLE 10

MEAN RADIAL VELOCITIES AND EQUIVALENT WIDTHS IN OCTOBER 2001

Line ID (1)	RV km s^{-1} (2)	GFWHM km s^{-1} (3)	EW (Å) Å (4)
H I			
4340.47	-26	250	0.9
4861.33	-39	200	0.9
HeI			
4387.93	-20	220	0.52
4471.58	-30	200	1.06
4713.26	-17	150	0.38
4921.93	-14	140	0.63
5015.68	-35	130	0.33
5875.80	-43	160	0.73
6678.15	-	150	0.85
C III			
4388.02	-36	166	0.51
N II			
5676.02	-12	100	0.1:
5679.56	-10	100:	0.23
O II			
4661.64	+3	50	0.16
5508.11	-14:	120	0.1:
Si II			
5219.37	-24	130	0.1:
Si III			
4552.62	-5	128	0.40
4567.83	-8	120	0.45
5739.73	-9	135	0.30
Mg II			
4481.23	-18:	140:	0.2

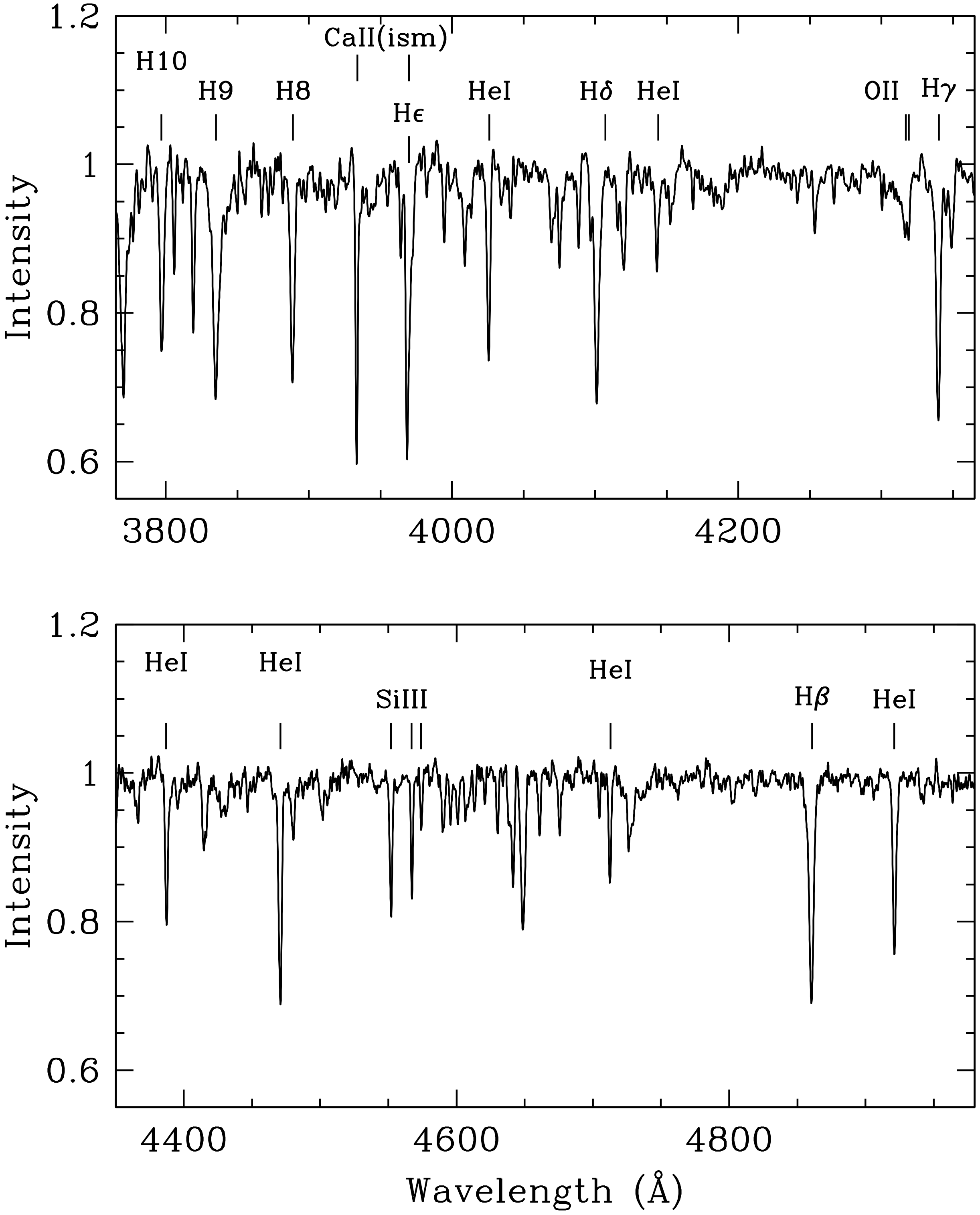

Fig. 1. A portion of the normalized spectrum of LS I+65 010.

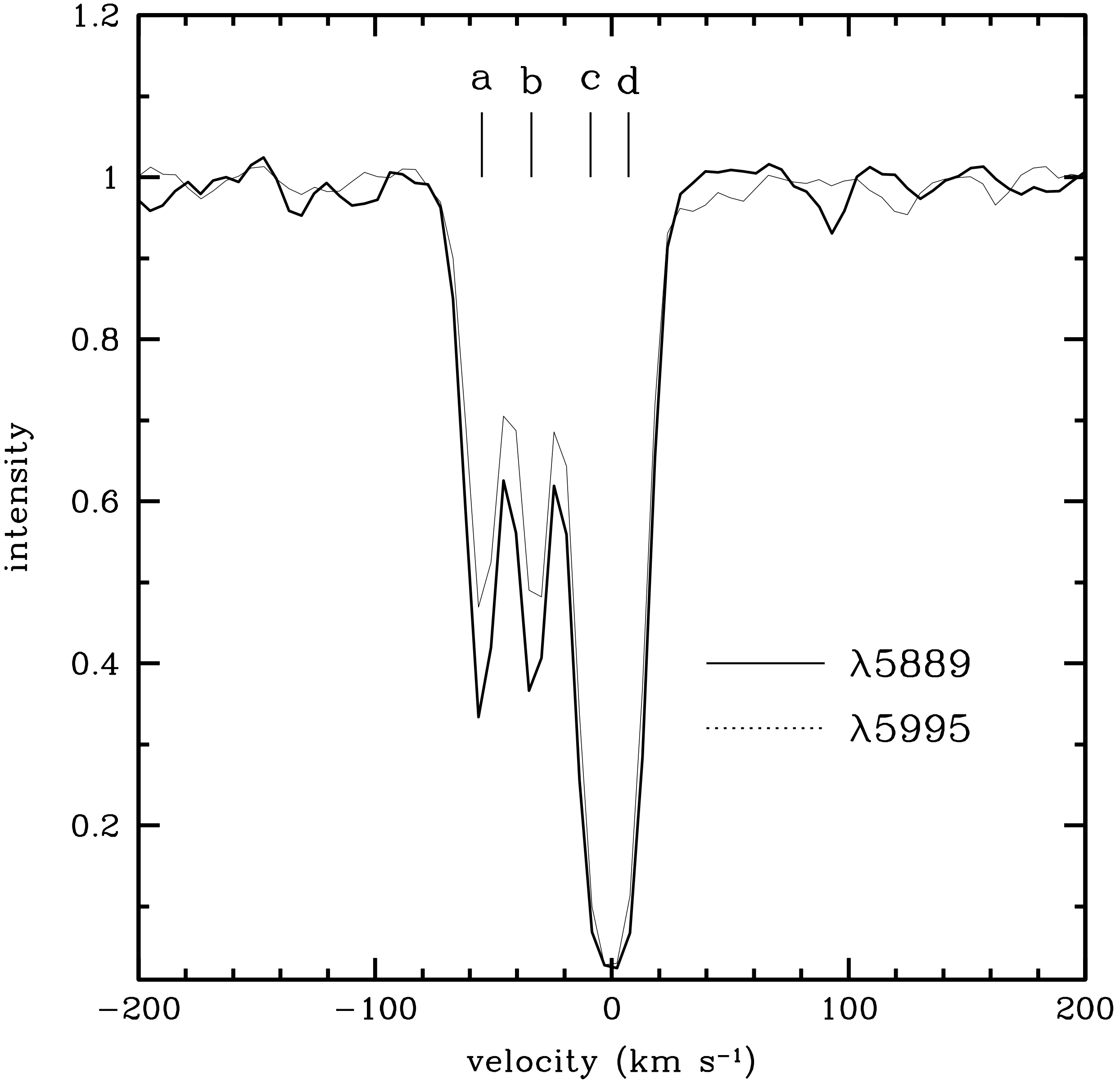

Fig. 2. Plot of the Na I $\lambda5889$ (dark) and $\lambda5895$ (light) line profiles observed in the coudé spectra of LS I+65 010. The tick marks indicate the central position of the four Gaussian profiles that were fit to the blend.

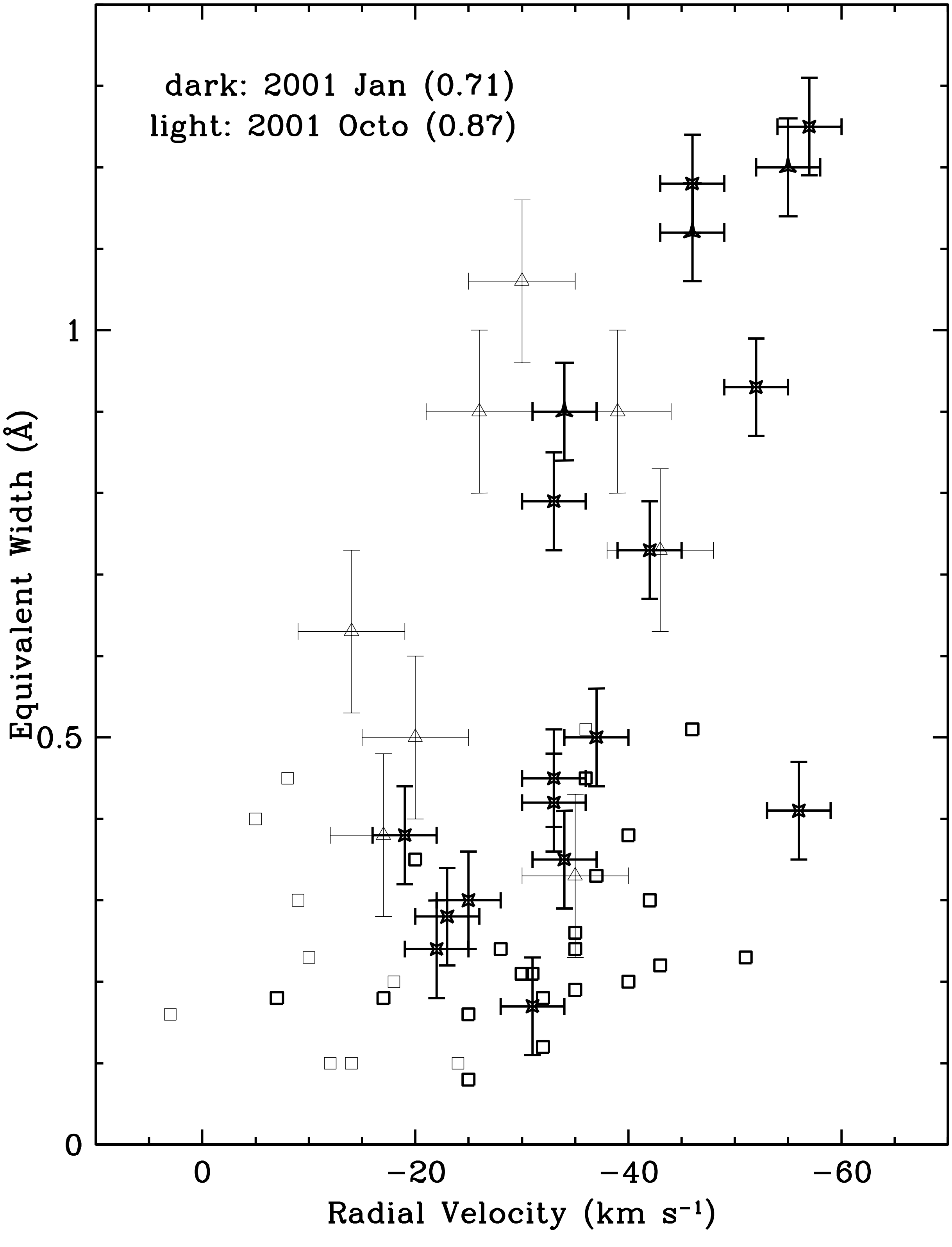

Fig. 3. Equivalent width of the photospheric absorption lines plotted against the velocity of the line, for the data of January 2001 (dark) and October 2001 (light). Triangles in the January data represent H-lines while crosses represent He I lines. The open squares represent lines from heavier elements (see Tables 8 and 9).

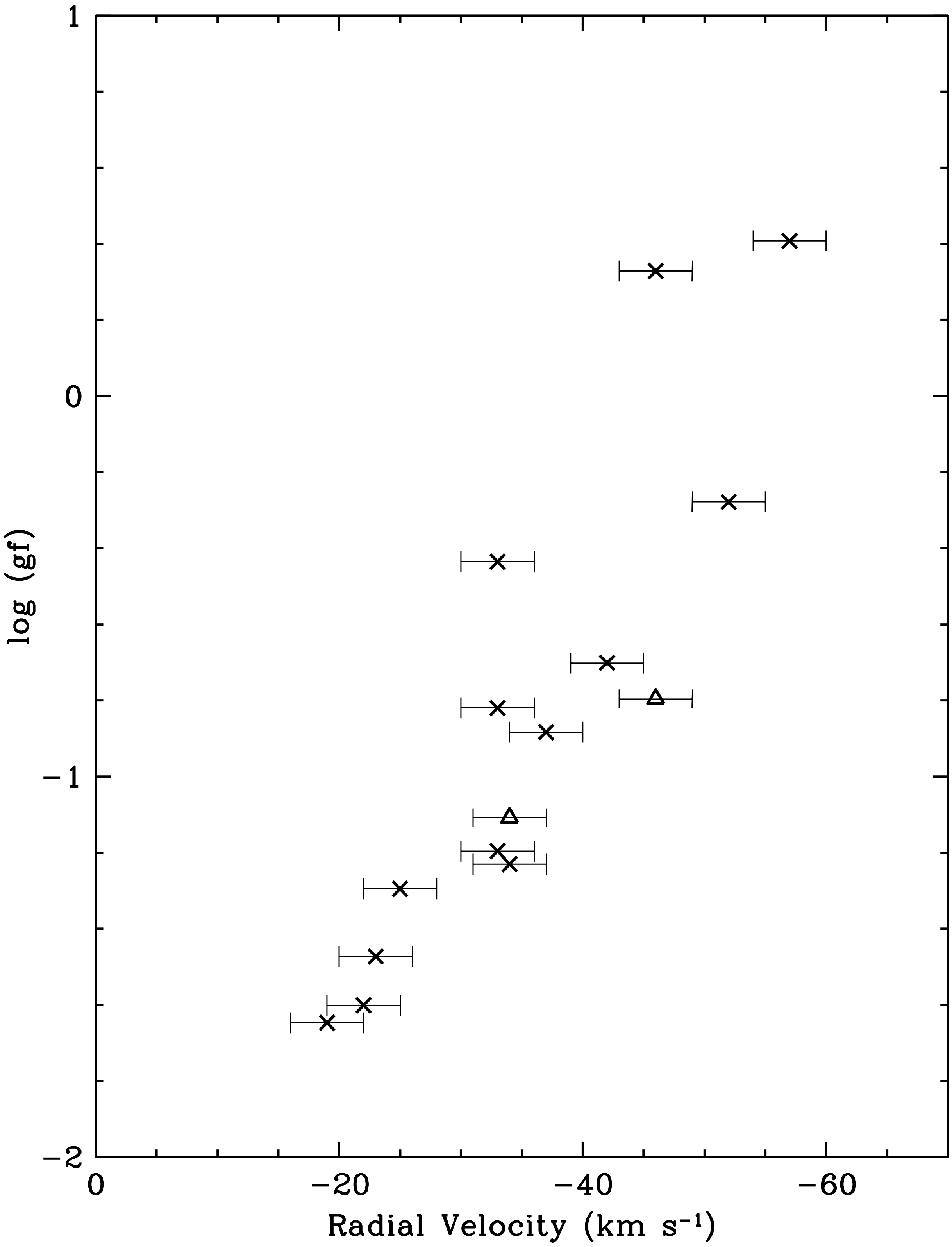

Fig. 4. Correlation of log(gf) *vs.* RV for the H and He I lines in the 2001 January data.

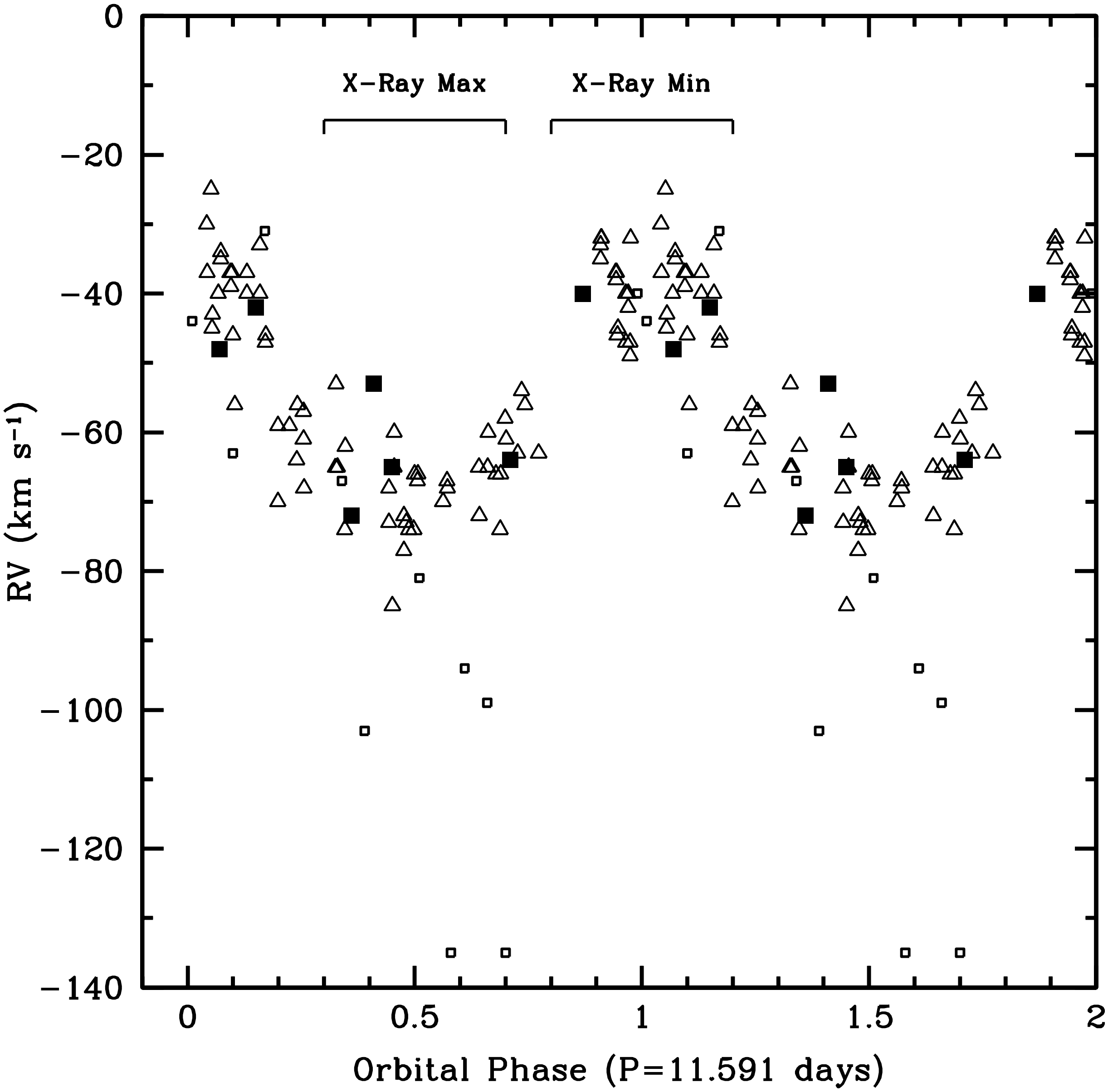

Fig. 5. Radial velocities folded in phase with the 11.591 day orbital period. Open triangles are the data of Crampton et al., open squares are the data published by Reig et al. for He I 6678, and filled squares are our Vel^{One} data for He I 5875 Å. Indicated are the approximate phase intervals during which the RXTE X-ray counts were maximum and minimum (from Fig. 7 of Corbet et al. 1999). The neutron star is "in front" at phase 0.25.

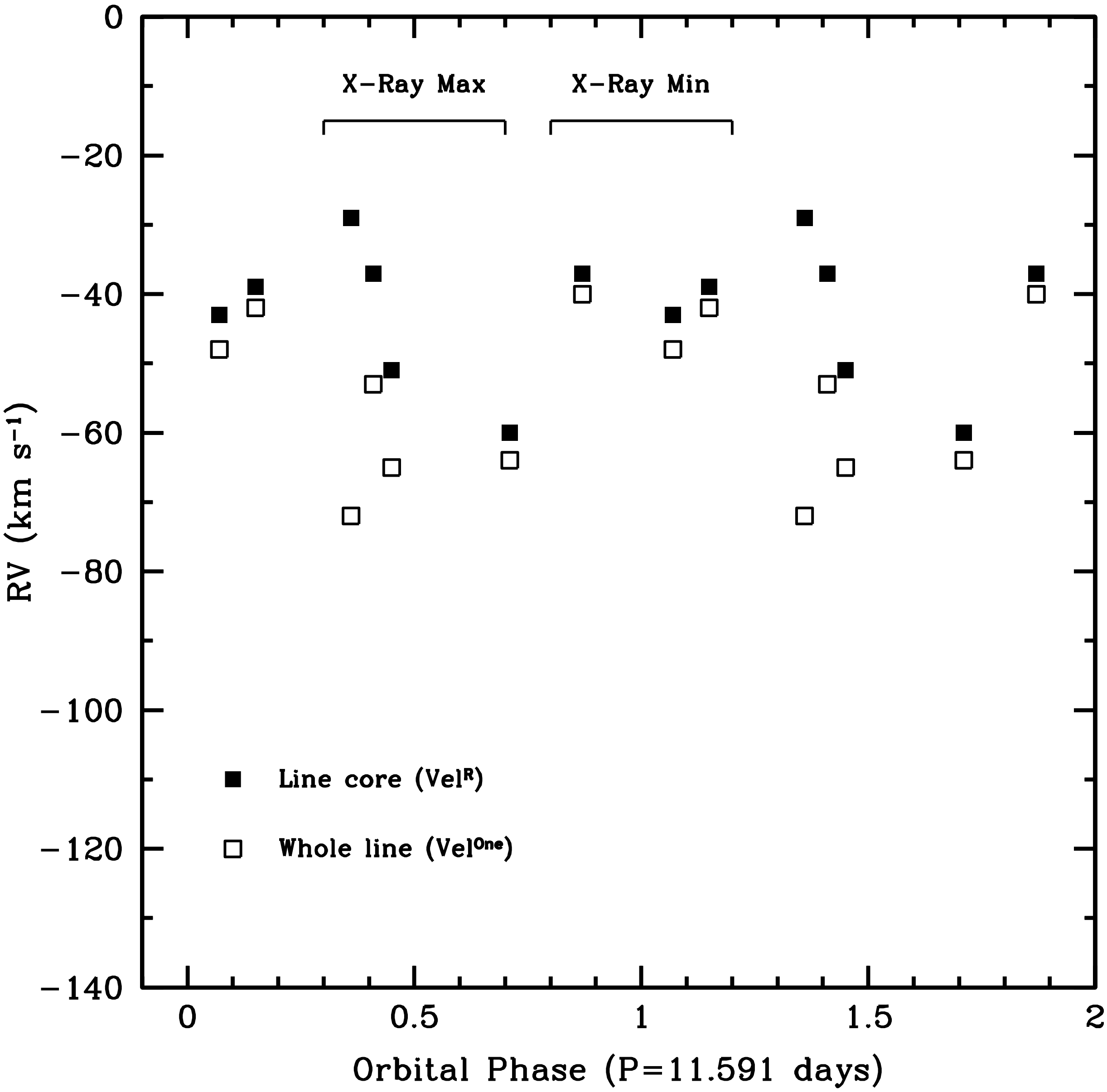

Fig. 6. Radial velocities of He I 5875 Å folded in phase with the 11.591 day orbital period: results obtained by measuring the whole line, using a single Gaussian fit (Vel^{One}; open squares) compared with the measurements of only the line core (Vel^{R}; filled-in squares). The two measurements have their largest discrepancy at phases when the X-ray flux is maximum.

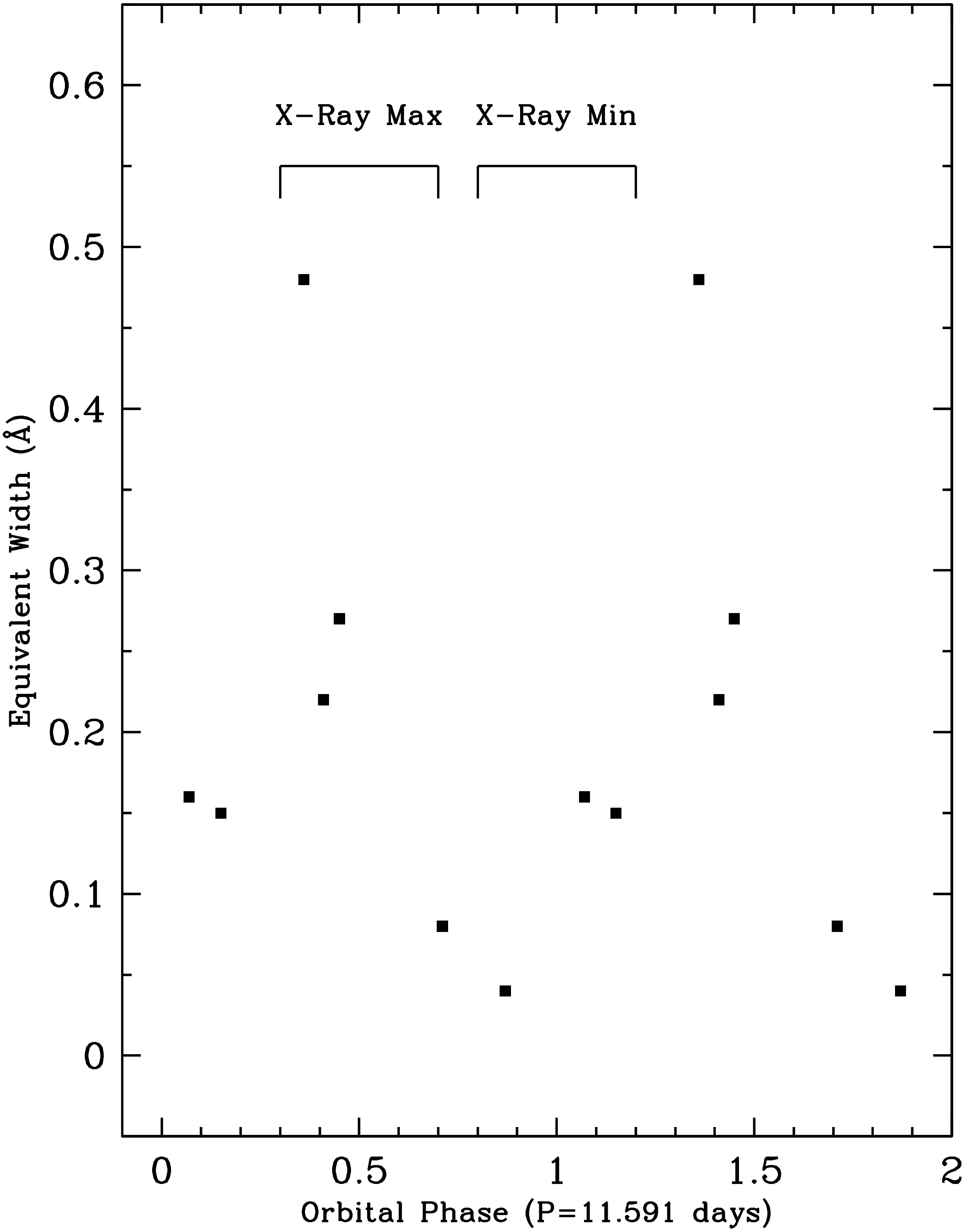

Fig. 7. Equivalent width of the "blue" Gaussian that was fit to the He I 5875 line profile, as a function of the 11.591 day orbital phase.

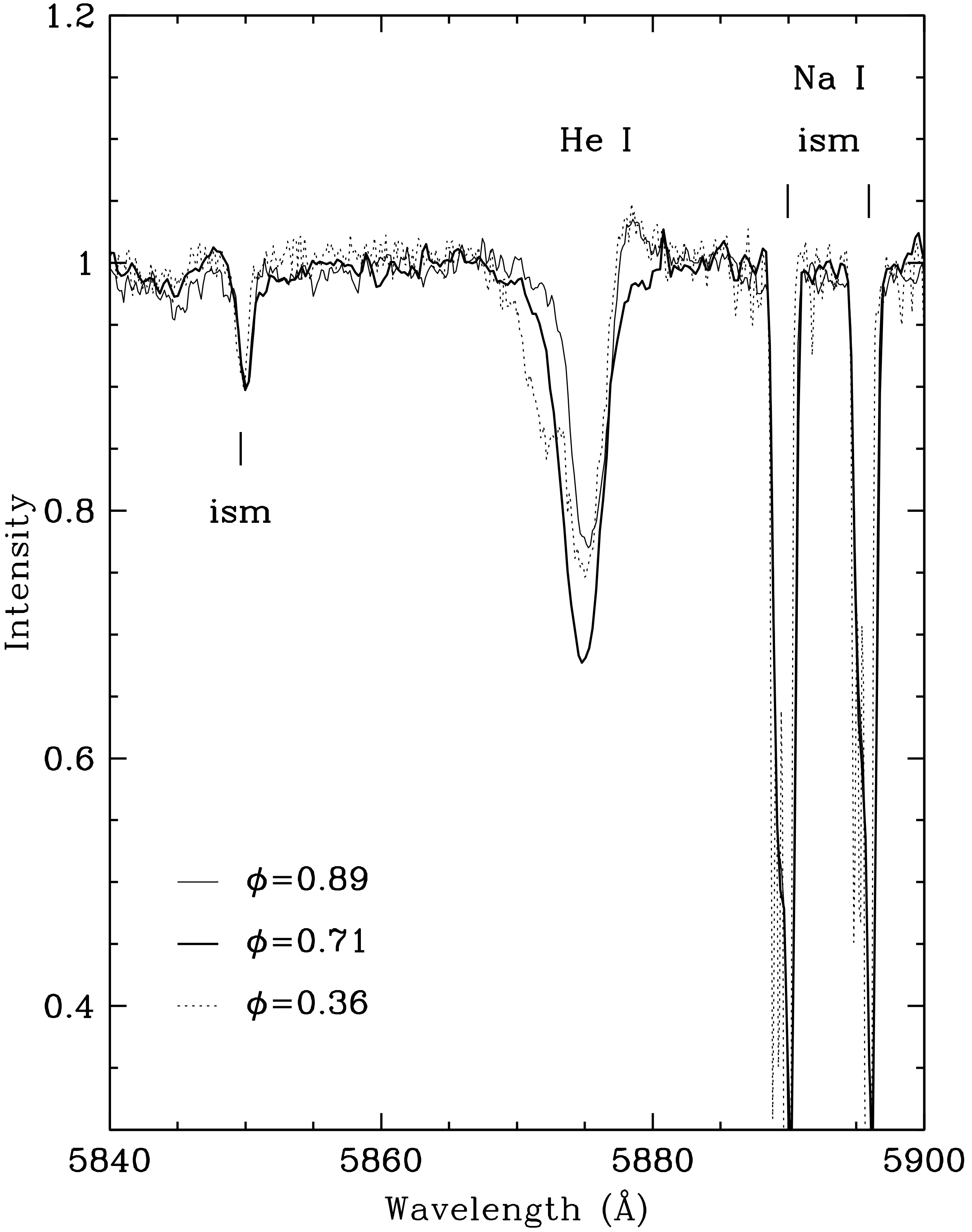

Fig. 8. Comparison of the He I 5875 line profiles at different orbital phases, as indicated. At orbital phase 0.71 (dark tracing), the collapsed object is on the far side of the B1-star, and the photospheric absorption line is deeper and more symmetric than at other phases.

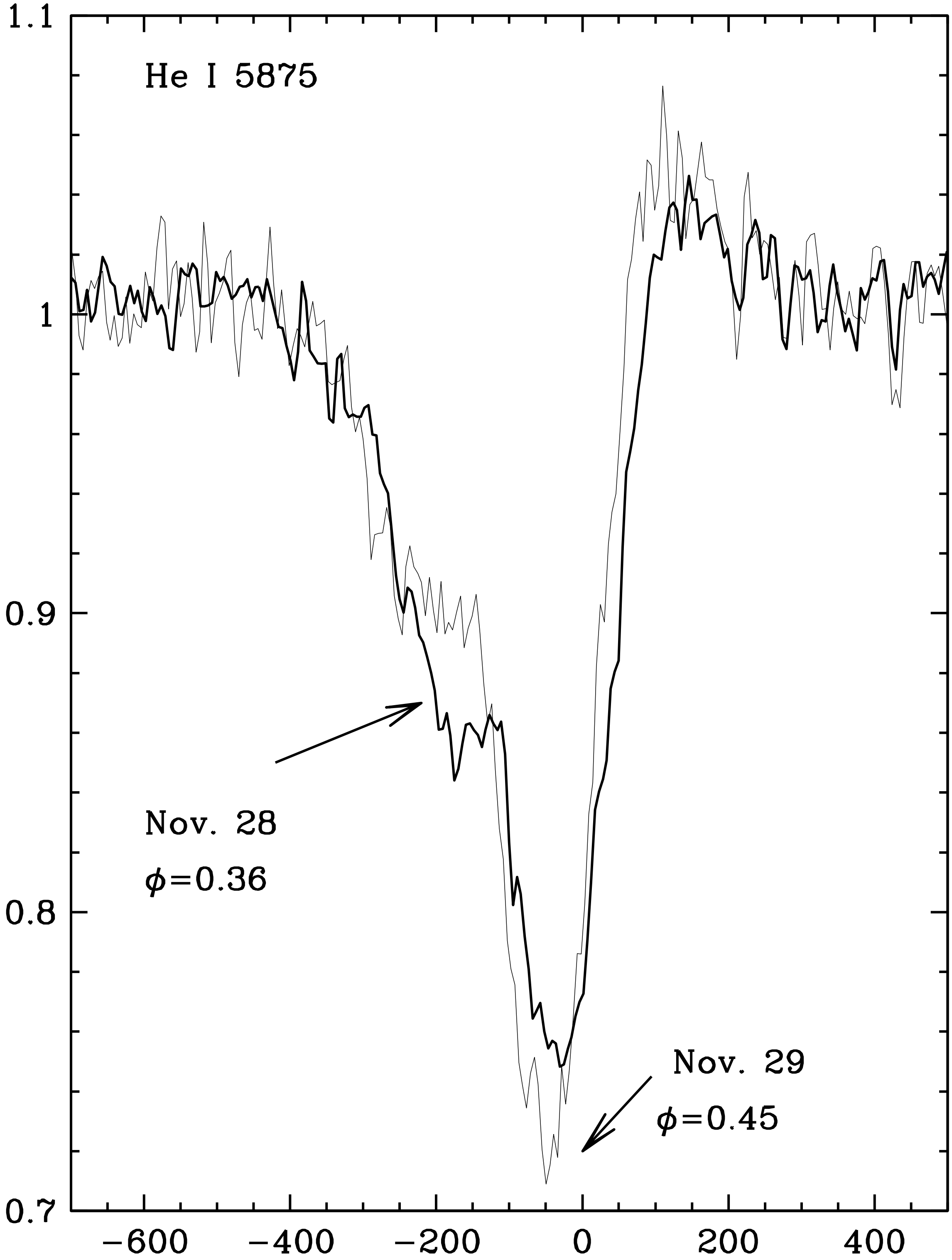

Fig. 9. Comparison of the He I 5875 profiles in the 1995 coude data. Note that the core of the line profile of 29 Nov. (dotted tracing) is displaced blueward with respect to the line profile of the previous night by 16 km s^{-1}.

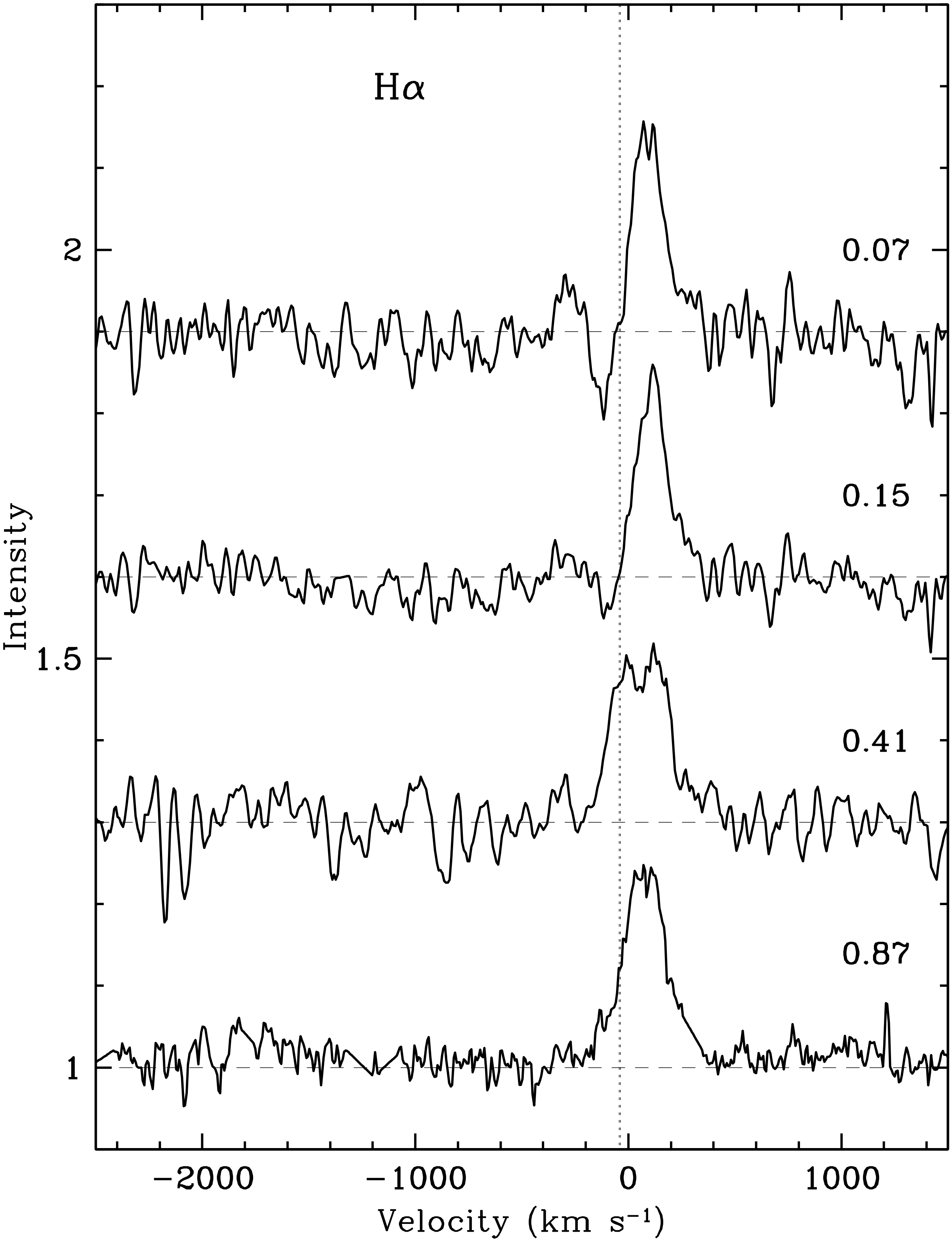

Fig. 10. Comparison of the Hα line profiles at different orbital phases, as indicated.

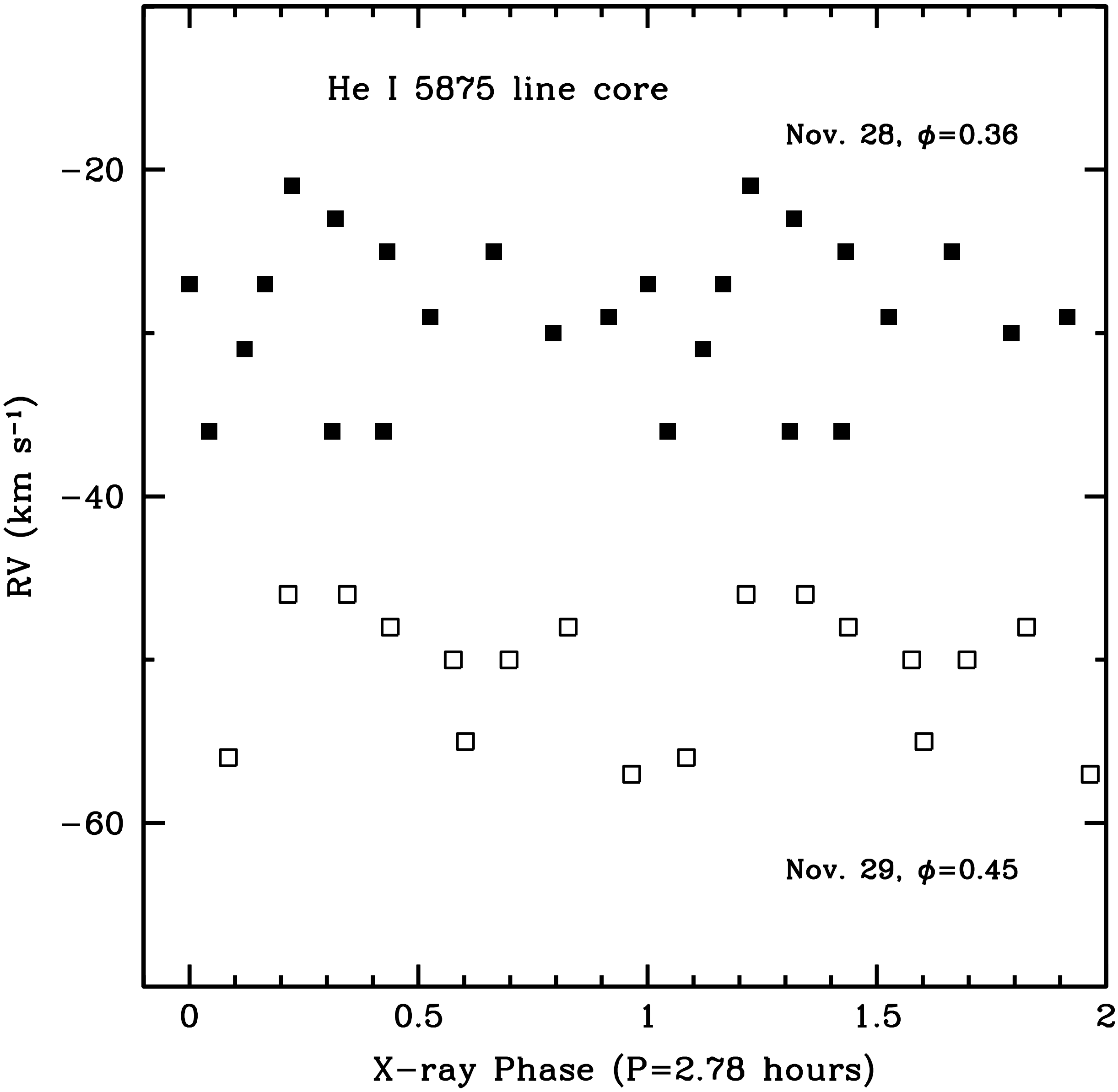

Fig. 11. Radial velocity of the "red" Gaussian (i.e., fit to the line core) of the He I 5875 absorption line in the 1995 data, plotted against 2.78 hour X-ray phase. Filled squares are Nov. 28 data and open squares are Nov. 29 data. Although variability is present on the short-term, it does not appear to follow the 2.78 hour X-ray flaring period.

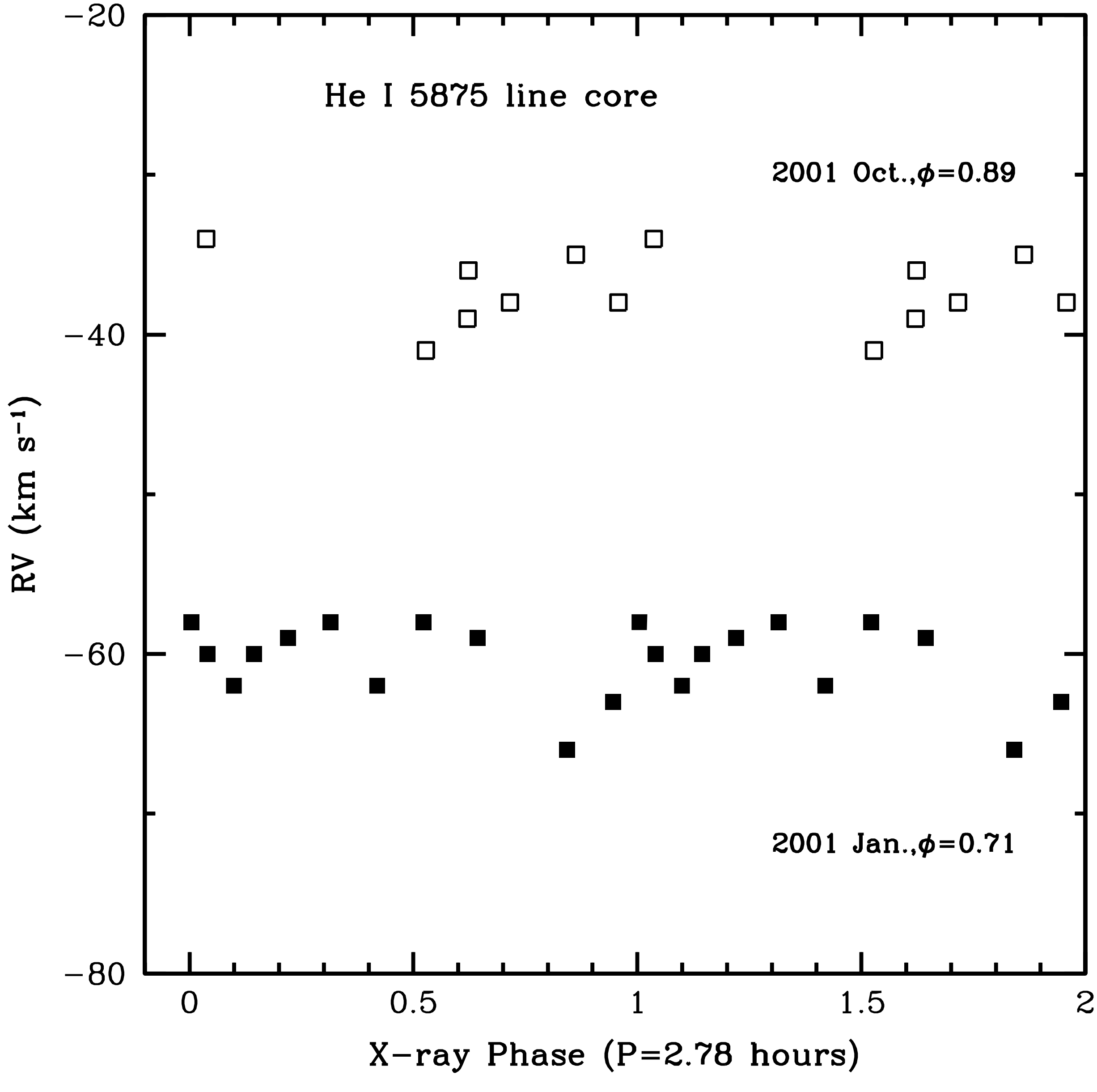

Fig. 12. Radial velocity of the "red" Gaussian (i.e., fit to the line core) of the He I 5875 absorption line in the 2001 data, plotted against 2.78 hour X-ray No variability greater than the ±5 km s^{-1} uncertainties is present. phase.

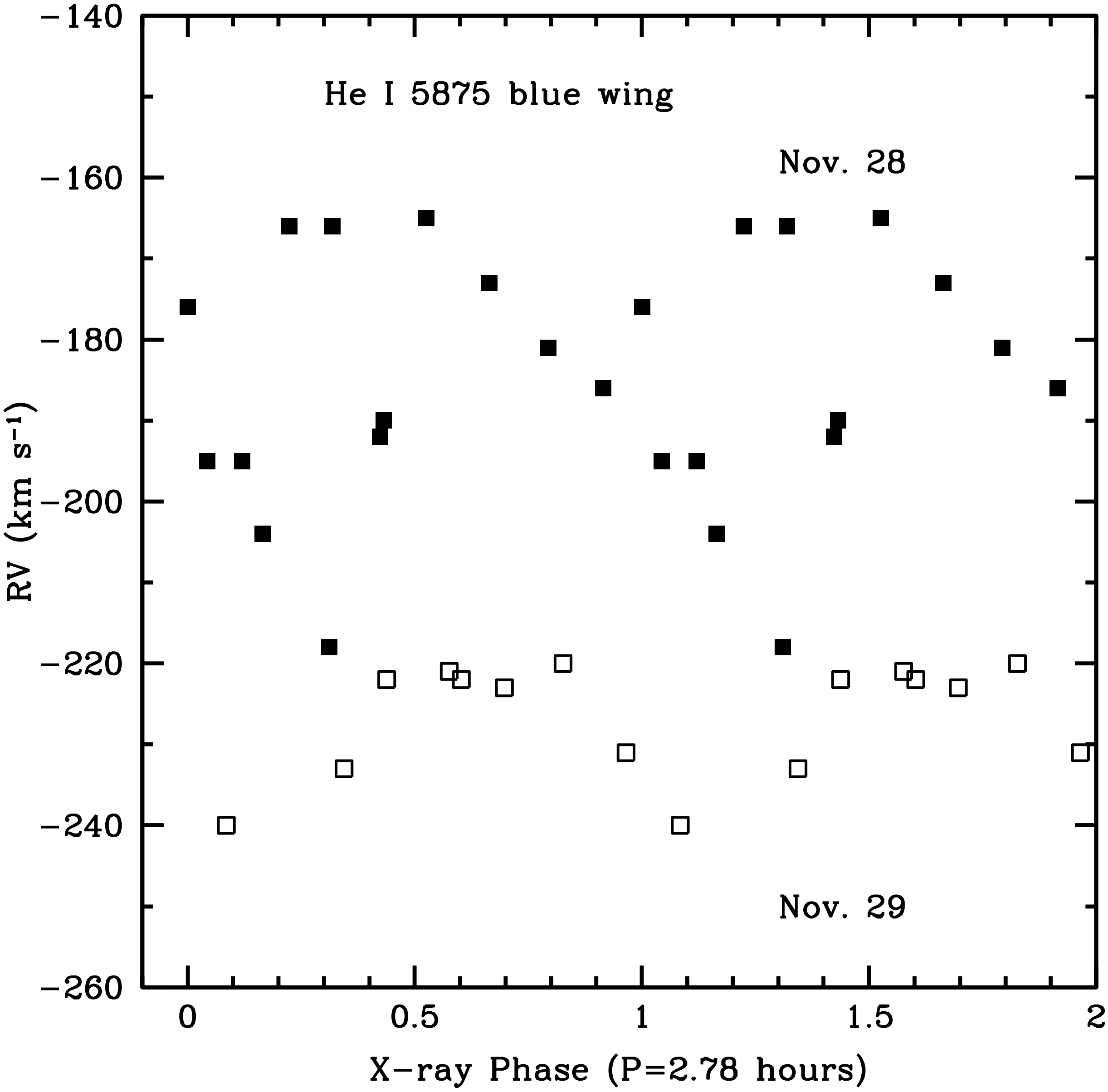

Fig. 13. Radial velocity of the "blue" Gaussian (i.e.,fit to the blue line wing) of the He I 5875 absorption line in the 1995 data, plotted against 2.78 hour X-ray phase. Filled squares are Nov. 28 data and open squares are Nov. 29 data.